End of Project Report - IRPA Long Term Project (7th Malaysian Plan)

Aerodynamic , Materials and Vibration Characterization for New Eagle Aircraft: Computer Modeling and Simulation

Research Team Members:

Dr Zaidi Mohd Ripin
Dr Roslan Ahmad
Dr Mohd Zulkifly Abdullah
Associate Professor Zoeb Husain

School of Mechanical Engineering
Unversiti Sains Malaysia
Kampus Kejuruteraan
14800 Nibong Tebal SPS Pulau Pinang

Acknowledgement

The team involved in this research project would like to acknowledge the Ministry of Science, Technology and The Environment for the research grant obtained from the IRPA programme without which this research would not be possible. We would also like to acknowledge the full support and encouragement received from the Universiti Sains Malaysia in the ceaseless drive for research inculturation. Our thanks to the Dean of School of Mechanical Engineering Prof Madya Dr Zainal Alimuddin for the full support allowing us the use of the wind tunnel and the computer facilities. Special mention must be given to the role of CTRM and Eagle Aircraft in this project without which this project could never started. Mr Tim Burton and Mr George Blower deserves special mention for their willingness to share their expertise and Encik Zulkarnain for his delivery of the keynote address and the encouragement given.

We are also grateful to our research students, notably Azurain for her involvement in this project, Chong Shah Leong and Yap Tze Chuan for their patience and endurance, all of who have been crucial in this research work. We would also like to express our sincere gratitude to all fellow researchers form UTM, UPM, UIA, UKM and KUITHO for their support throughout this project.

Finally, we would like to dedicate this report to Prof Madya Dr Zoeb Husain who is presently undergoing treatment after a heart bypass surgery. He has been instrumental in initiating this work and has inspire us to work harder and to take Eagle into the wind tunnel and the CFD simulation.

Thank you

Dr Zaidi Mohd Ripin
Dr Mohd Zulkifly Abdullah
Dr Rosaln Ahmad
Prof Madya Dr Zoeb Husain

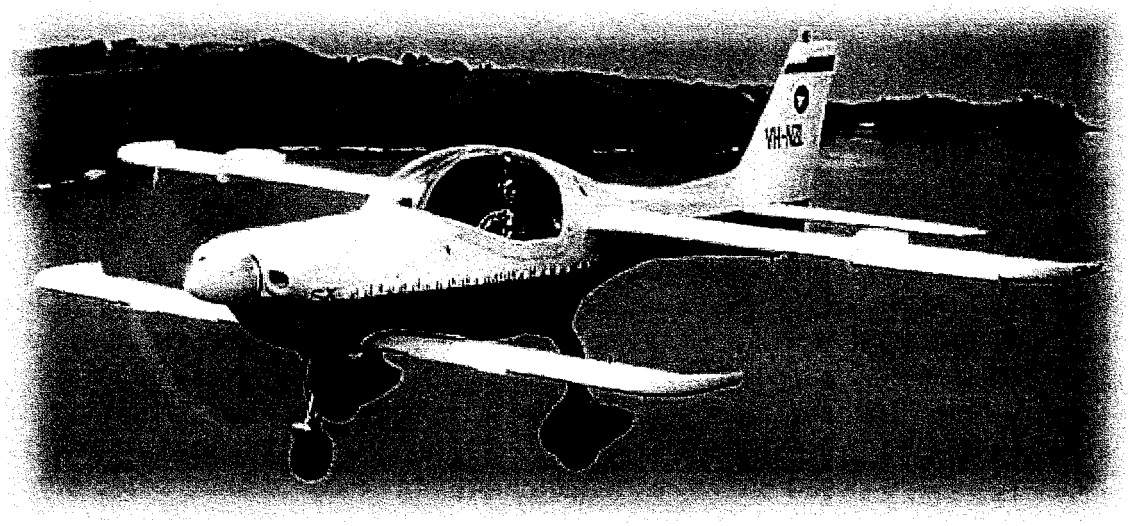

Figure 1 - Eagle 150 photo. The small front wing is known as canard. All full CRP construction this small Australian design and Malaysian made aeroplane is the subject of this research work under this IRPA Grant.

The comprehensive of the research plan was because the approach adopted was a system approach and to develop the indigenous capability in aircraft analysis based on current baseline design which will allow future upgrade and modification to be carried out based on the existing design. Interview with the Eagle Aircraft (M) Sdn Bhd Managing Director (Mr George Blower) indicated that Eagle 150 was waiting for certification for Federal Aviation Authority (FAA) in the United States of America, the certification of which will allow further market penetration by Eagle into the highly comptetitive US and NAFTA market. From the interview also it was recognised that whatever experimental and simulation data available on Eagle would be helpful in promoting this aircraft. Since the aircraft is build locally then the research would make the characterization of the aircraft as its main objective and this leads to the two major steps in the plan which includes experimentation and simulation.

Why experimentation?

Research carried out by Dr Roslan [Thesis, papers] indicated that the data on measured strength on composite specimens have wide range of values upto 40 percent discrepancies, unlike metal for example mild steel the Young's modulus remains around 200 GPa. Therefore there is an urgent need to identify whether the variations in the strength of the composite component build by CTRM existed and if it exists by how much? The only way to find this is to measure the strength of the specimens obtained from CTRM thorughout the research period in order to map the variation of strength in production. The suggested experiments included tensile tests and also dynamic loading test to ascertain impact strength of the specimen. The build up of database from this work will

The research plan was comprehensive and it covers the major areas of the Eagle aircraft design. The team was hoping that Eagle can be characterized and understood. The budget includes the buying of data logger, vibration analyser and improved instrumentation for the existing wind tunnel in USM which amounts to RM 1 020 450. Upon submitting the proposal, the approved research grant was RM 198 000 which is 19% of the original proposal. With this budget the whole plan has to be reviewed and downsized, therefore the work was limited to investigate the general aspect of aerodynamics, vibration and impact strength characterization by computer simulation alone.

2.0 Research Work

2.1 Aerodynamic studies of Eagle

Experimental Work

in this study, the Eagle is treated as small low speed aircraft used as surveillance, recreational or as trainer aircraft where the wings are designed for high lift and low drag at relatively low Reynolds number. The cross section of the Eagle wing airfoil was subjected to wind-tunnel measurement using the low speed open circuit tunnel facilities available in the School of Mechanical Engineering, Universiti Sains Malaysia where the Reynolds number tested were up to 2.25×10^5.

The results showed that the canard has greater lift coefficient than the wing and that both stall at almost the smae angle of attack. Use of flaps to full defelction of 35 degrees increases the lift coefficient of wing and canard by 31 percent and 50 percent respectively. At all flap deflection angles, canard and wing stall at lower angle of attack as compared to clean airfoils.

The overall performance is good and shows marked resembleance with the typical characteristics of NACA airfoils. A typicaly lift curve for both canard and wing showed that stall does not occur so suddenly as compared to the conventional NACA airfoils which is the reason why the airfoils have been tailor made: so as to serve the aircraft own requirements parallel to the unique design of the aircraft. The disadvantage of the rapid stall NACA airfoil to a tandem wing design aircraft like the Eagle is that the take off and landing angle would be steeper than desired, producing positive pitching. The detail of this research investigation is reported in the Journal of Institution of Engineers Malaysia, 2001 [1].

Computational Fluid Dynamics (CFD) Simulation

Using comercially available CFD software fluent 5.5, the aerofoil measured earlier was simulated for Reynolds number of 2.25×10^5. The lift and drag

coefficients determined by varying the angle of attack from 0-16 degrees and the use of flaps to full deflection of 35 degrees increases the lift coefficient of the wing and canardto 37.5% and 55% respectivley. However when compared to experimental data, the lift coefficient obtained by simulation is higher as the losses has not been fully considered (inviscid flow). This shows the limited and the need to verify the CFD simulation with experimental data. The full description of the work is presented in the Proceedings of the National Conference on Aerodynamics and Related Topics ART 2001.

2.2 Wind induced vibration

The wind induced vibration is one of the problem faced for long span of wings which is not a major problem for small aircraft like the Eagle 150. However this area is very difficult since the analysis involves transient phenomenom. In this study a simulation study was carried out on vibration of circular cylinder in wind induced vibration so that analysis of the full wing vibration can be carried out in the future. Analysis of wind or flow induced vibration was carried out using the FEMLAB programme which solves the unsteady flow analysis over a circular cylinder. The time-varying pressure distribution on the object and the resulting motion within the fluid flow is the objective of this study. The research started with the study of relatively simple one degree of freedom model where it is subjected to time-varying force associated with either the displacement or the velocity or the acceleration of the object based on the findings of other researchers. However the implementation of such forces (either linear or non-linear) do not result in satisfactory outcome. Comparativelt the best method comes from the drag force made as a function of time, sinusoidally varying according to Strouhl frequency. The results obtained are comparable with other published results. The work then extends to include the analysis of pressure distribution around a cylinder for unsteady flow usng MATLAB and CFD-FEM model (FEMLAB) and the drag forces determined over time for static and moving cylinder. The results showed the approach is able to predict the time varying drag forces and the vortex frequency does not vary much for static and moving cylinder. The detail aspect of the work is presented in the Proceedings of the National Conference on Aerodynamics and Related Topics ART 2001.

2.3 Impact analysis of composites

One of the important apsect of this study is to look into the behaviour of the carbon composite (carbon reinforced plastics- CRP) when subjected to dynamic loading since the material is used in the construction of the fuselage and the wings. The difficulty in this modeling work is the non-linear nature of the material and the nature of dynamic loading. Based on research on impact loading, it was decided that at this level it is premature to study the whole body response (Eagle 150) on dynamic loading, in particular in a crash landing sceanrio where the structural integrity can be ascertained and measured. A preliminary study was

intiated to look into the application of PAM SHOCK in replicationg the experimental data of CRP tubes but the results was less discouraging. The full description of the work which forms the basis of the study is presented in the Proceedings of the National Conference on Aerodynamics and Related Topics ART 2001.

3.0 Research Outcome

The outcome of this research can be measured in four major criteria which includes the papers published, manpower development which includes postgraduate training and technicians skill development, technology transfer in terms of research findings dissemination and the establishment of industrial and academic linkages. In this section the details form each deliverables are reported.

3.1 Papers published

There are 4 papers published from the research work carried out directly related to the Eagle 150 and the associated technology (material wise and also operational wise). The papers are listed below:

1. A. Jaafar, ZM Ripin, MZ Abdullah, R Ahmad and Z Husain, " Aerodynamic Characteristics of Canard Wing of Low Speed Aircraft", Journa of Institute of Engineers Malaysia, Vol 62, No.2, June 2001, pp 3-8

2. Z Husain, MZ Abdullah and TC Yap, "CFD Simulation and Aerodynamics of Low Speed Tandem Wing Design Aircraft", Proceedings of the National Conference on Aerodynamics and Related Topics ART 2001, Penang, ZM Ripin et. al. Ed., pp. 1-11

3. ZM Ripin and CS Leong, "Analysis of Flow Induced Vibration", Proceedings of the National Conference on Aerodynamics and Related Topics ART 2001, Penang, ZM Ripin et. al. Ed., pp. 101-112

4. R Ahmad and MR Said, "Buckling Analysis of Composite Tubes Due To External Radial Impulsive Loading" , Proceedings of the National Conference on Aerodynamics and Related Topics ART 2001, Penang, ZM Ripin et. al. Ed., pp. 148 - 161

5. A.Jaafar,Z.Husain,Z.Mohd Ripin,M.Z.Abdullah,"Aerodynamics and Characteristics of Canard?wing of Low Speed Eagle Aircraft",Int. Conf. of Advanced Strategic Technologies, Kuala Lumpur, August 14-17, 2000

6. T.C. Yap, M.Z. Abdullah, Z. Husain , Z. Mohd Ripin, R. Ahmad, "The effect of turbulence intensity on the aerodynamic performance of airfoils", 4th Int. Conf. on Mechanical ENgineering, Dhaka, Bangladesh, Dec. 26-28, 2001

3.2 Postgraduate Training

In terms of human resource development, the clear tangible output is the number of postgradute research in this project. There were three postgraduate students involved in this project and they are listed below:

1. Azuraien Jaafar, PhD candidate
2. Chong Shah Leong, MSc, graduated 2001
3. Yap Tze Chuan, MSc, graduated 2001

There are other intangibles such as the development of the technicians who are involved in this project in particular the setting up of the wind tunnel for model aircraft experimentation and the sourcing out of model building in Malaysia. The Eagle 150 model (scale model of 1:25) was made by local artisan which paves the way for more complex model testing in the future.

3.3 Technology transfer

Technology transfer was one of the main activities in this research work. During the project a lot of discussions were made with CTRM and it is with their assistance that the scale model of the Eagle 150 was successfully built and experimented. The detail laboratory data was submitted to the Eagle aircraft management for their perusal and it is with their support that this project finally took off.

Another activity which was one of the major success of this project is the National Conference on Aerodynamics and Related Topics (ART) 2001 which took place in the Engineering Campus, Universiti Sains Malaysia, Transkerian. The conference which is the first of its kind in Malaysia, specifically targeted the aerodynamics area and the aerospace industries to sit together and to keep up to date with the latest development in Malaysia regarding the overall aerospace and aeronautical industries. The guest speaker was Dr Ahmad Sabirin Arshad of Astronautic Technology Sendirian Berhad (ATSB) the national company responsible for developing the first Malaysian made satellite the Tiungsat-1 and Encik Zulkarnain from the Composite Technology Research Malaysia Berhad the national company spearheading the development of aircraft assembyl and manufacturing in Malaysia. There were 14 papers presented orally and in poster form and with more than 30 participants, the conference was considered a

resounding success and can be a model of technology transfer in IRPA funded project.

3.4 Industrial and Academic Linkages

The strength of the research work was also the identification of the School of Mechanical Engineering as one of the resource centre for aircraft studies. By carrying out this project the team members were able to carry out these important duties:

i) Identifying major pockets of aerospace research in Malaysia. Visits to UKM, UPM, UTM and ITM inidcated limited human resource in research in aircraft development.

ii) Identifying and establishing working relations with the two major aerospace companides in Malaysia, namely CTRM and ATSB. Until today, the relationship is sustained and groundwork preparation is being made for further deeper reseach and development work with these companies.

iii) Identifying major assets for reseach in aerospace and aeronautical, for example the Low Speed Wind Tunnel facilites , the biggest and most comprehensive in Malaysia is made known through this linkages and the ART 2001 conference made possible through this research.

4.0 Assets acquired

Through this project major asset acquistions made are listed below

1 unit of SUNSparc Workstation with Ultrasparc 200 MHz Processor with 512 MB RAM and 20 GB Hardddisk come with 19" monitor
1 unit of SUNSparc Workstation with Ultrasparc 100 MHz Processor with 256 MB RAM and 10 GB Hardddisk come with 19" monitor
1 unit of DELL PC Workstation with Intel Pentium III Processor with 512 MB RAM and 20 GB Hardddisk come with 19" monitor

These workstations were used to run Fluent V5.0 software for simulation, ANSYS finite element method software, FEMLAB software and PAM SHOCK software which are the main tools used in this research. The softwares were leased annually from the associated suppliers using the grant.

APPENDIX I

LIST OF PAPERS :

1. **AERODYNAMIC CHARACTERISTICS OF CANARD WING OF LOW SPEED AIRCRAFT**

2. **CFD SIMULATION AND AERODYNAMICS OF LOW SPEED TANDEM WING DESIGN AIRCRAFT**

3. **ANALYSIS OF FLOW INDUCED VIBRATION**

4. **BUCKLING ANALYSIS OF COMPOSITE TUBES DUE TO EXTERNAL RADIAL IMPULSIVE LOADING**

5. **AERODYNAMICS AND CHARACTERISTICS OF CANARD WING OF LOW SPEED EAGLE AIRCRAFT**

6. **THE EFFECT OF TURBULENCE INTENSITY ON THE AERODYNAMIC PERFORMANCE OF AIRFOILS**

IEM Council Session 2001/2002

President:
Ir. Dr. Gue See Sew

Deputy President:
Ir. Prof. Abang Abdullah Abang Ali

Vice Presidents:
Ir. Peter Chong Chung Ping
Ir. Vincent Tan Heng Kui
Ir. Assoc. Prof. Ruslan Hassan
Ir. Prof. Haron Ismail
Ir. P.E. Chong
Ir. Vincent Chen Kim Kieong

Immediate Past President:
Y. Bhg. Datuk Ir. Prof. Dr. Hj. Ahmad Zaidee Laidin

Past Presidents:
Y. Bhg. Tan Sri Ir. (Dr.) J. G. Daniel, Y.Bhg. Dato' Ir. Pang Leong Hoon, Ir. Hj. Mohd Mazlan, Ir. P.E. Chong, Ir. Dr. Ting Wen Hui

Hon. Secretary:
Ir. Lee Weng Onn

Hon. Treasurer:
Ir. Oon Chee Kheng

Council Members:
Civil Representatives - Ir. Lim Ah Hang
Mechanical Representatives - Ir. Aw Kong Koy
Electrical Representatives - Ir. Yusouf Ahmad
Structural Representatives - Ir. Mohd. Salleh bin Mohd. Noh
Chemical & Other Representatives - Ir. Dr. Tee Tiam Ting

Members:
Ir. Mohd. Aman bin Hj. Idris, Ir. Prof. Madya Dr. Rosli bin Hamir, Ir. Assoc. Prof. Siti Hawa bte Hamzah, Ir. Prof. Dr. Radin Umar Radin Sohadi, Ir. Assoc. Prof. Dr. Hasanan bin Md. Nor, Ir. Awangku Hidup bin Awangku Hosain, Ir. Dr. Wong Fook Keong, Ir. Chin Mee Poon, Ir. Prof. Dr. Wan Mahmood Wan Abdul Majid, Ir. Capt. Sukdev Singh, Ir. Prof. Dr. Ow Chee Sheng, Ir. Prof. Ishak bin Abdul Rahman, Ir. Ms. Toh Yuan Kait, Ir. Chee Meng Sang, Ir. Abdul Rahim bin Haji Othman, Ir. Yim Hon Wa, Ir. Dr. Ahmad Fadzil bin Hj. Mohamad Hani, Ir. Low Ah Peng, Ir. Norlida bte Buniyamin, Ir. Ooi Kah Huat, Ir. Cheng Chee Song, Ir. Muhammad Guntor Mansor Tobeng

Branch Representatives:
Northern - Ir. Chong Chee Yoong, *Southern* - Ir. Puan Tak Hong, *Perak* - Ir. Dzulkarnain Kamaruzzaman, *Eastern* - Ir. Mohamad bin Husin, *Negeri Sembilan* - Ir. Loo Way Men, *Melaka* - Ir. Hj. Ahmad bin Tamby Kadir, *Sarawak* - Ir. Henry Foong Ah Ladd, *Miri* - Ir. Lim Leong Kee, *Sabah* - Ir. Andrew Amaladoss, Kedah-Perlis - Y.Bhg. Dato' Ir. Prof. Dr. Mohd Noor bin Salleh

Lembaga Pengarang:
Ketua Pengarang – Ir. Chin Mee Poon

Members of Standing Committee on Publications:
Pengerusi - Ir. Peter Chong Chung Ping,
Naib Pengerusi - Ir. Chee Meng Sang, Ir. Chin Mee Poon, Ir. Prof. Dr. Ow Chee Sheng, Ir. Lim Eng Hwa, Ir. Prof. Dr. Radin Umar Radin Sohadi, Ir. Dr. Abdul Aziz Samad, Ir. Dr. Eric Goh Kok Hoe, Ir. Ho Fong Seng, Sdr. Mohd. Rasid Osman, Ir. Assoc. Prof. Dr. Hasanan bin Md Nor, Ir. Low Ah Peng, Ir. Aw Kong Koy, Sdr. Kok Hee Poh, Sdr. Aaron Tan, Sdri. Jenifer Tan Yee Ying, Ir. Dr. Rosli Hamir

Content

VOL 62 No. 2 June 2001
KDN PP5476/7/2001 ISSN 0126-513X

International Advisory Panel

Prof. J.M. Owen, *University of bath, UK*
Prof. Don Mclean, *University of Southampton, UK*
Prof. Hiroshi Yabe, *University of Kyoto, Japan*
Prof. M. Rodds, *University of Wales, UK*
Prof. A.J. Saul, *University of Sheffield, UK*

Branches

Kedah - Perlis	: Universiti Pendidikan Sultan Idris, 35900 Tanjung Malim Perak Darul Ridzuan. *(Y. Bhg. Dato' Prof. Ir. Dr. Mohd. Noor bin Salleh)*	Tel : 05-458 2622 Fax : 05-458 2773
Northern	: c/o Kelab Ilham 225, Jalan Macalister, 10450 Penang. *(Ir. Choong Chee Yoong)*	Tel : 04-229 2045 Fax : 04-229 2045
Perak	: Institut Penyelidikan Galian, Jalan Sultan Azlan Shah 31400 Ipoh, Perak. *(Ir. Dzulkarnain bin Hj. Kamaruzzaman)*	Tel : 05-545 7104 Fax : 05-547 7185
Eastern	: Pejabat Pengarah Kerja Raya Negeri Pahang, Kompleks Tun Razak, Bandar Indera Mahkota, 25582 Kuantan. *(Ir. Mohamad bin Husin)*	Tel : 09-573 2040 Fax : 09-573 2837
Melaka	: 2, Jalan Malinja 2, Taman Malinja, Bukit Baru, 75150 Melaka. *(Ir. Hj. Ahmad b. Tamby Kadir)*	Tel : 06-284 8028 Fax : 06-283 8919
Southern	: 24B, Jalan Abiad, Taman Tebrau Jaya, 80400 Johor Bahru. *(Ir. Puan Tak Hong)*	Tel : 07-331 9705 Fax : 07-331 9710
Sabah	: 77-3, Wisma New Far East, Luyang, 88855 Kota Kinabalu. *(Ir. Andrew Amaladoss)*	Tel : 088-236 749 Fax : 088-236 749
Sarawak	: IEM Sarawak Branch, Ultimate Professional Centre, 2nd Floor, 16, Jalan Bukit Mata Kuching, 93100 Kuching Sarawak. *(Ir. Henry Foong Ah Ladd)*	Tel : 082-428 506 Fax : 082-243 718
Miri	: Lot 783, 2nd Floor, Bintang Jaya Commercial Centre. 98008 Miri, Sarawak. *(Ir. Lim Leong Kee)*	Tel : 085-412 900 Fax : 085-414 900
Negeri Sembilan	: 428, Jalan Tun Dr. Ismail, 70200 Seremban. *(Ir. Loo Way Men)*	Tel : 06-761 9211 Fax : 06-761 9511

Online Malaysia BBS Tel. No: 03-292 4177 - IEM Confer...

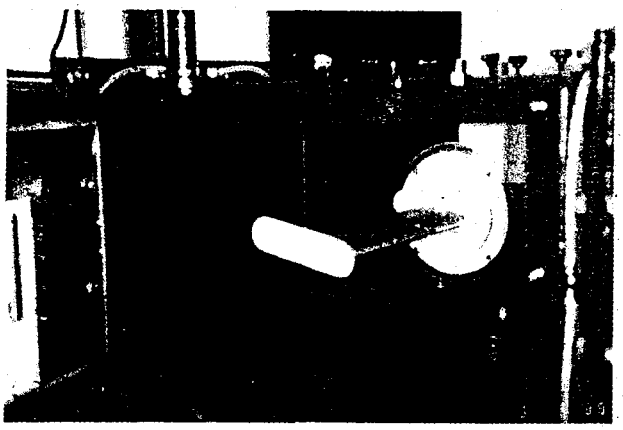

Figure 4 : Eagle air foil mounted in the wind tunnel test section

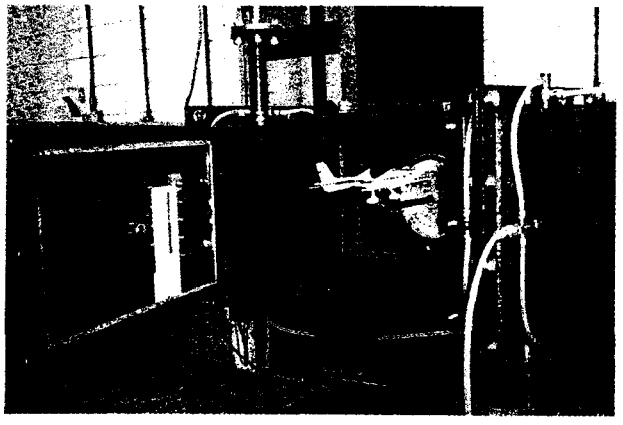

Figure 5 : Eagle 150 model mounted in the wind tunnel test section

angle decreases from 11° to 9°. The maximum value of lift at full deflection is 2.0. Again at zero angle of attack, for full flap deflection, the lift coefficient increases by 5 times as compared to a clean flap. Thus, the experimental results show that both the airfoils behave very similar aerodynamically.

Figure 9 shows a relationship between $C_{L_{max}}$ and flap deflection for the wing and Figure 10 is for the canard. The curves for both airfoils are identical. For the wing, there is a 31.25% increase in $C_{L_{max}}$ at flap angle of 35°. The increase in lift coefficient is linear up to flap angle of 20° and is curvilinear, subsequently. The increase in lift coefficient from 20° to 35° is only 10%.

Figure 11 and 12 give the performance of the airfoil of the wing and canard respectively. At zero flap deflection angle, the ratio of $CL/CD \approx$ 11- 12 for both airfoils. It decreases with increasing angle of attack and behaves as a blunt body near stall.

Based on. the values of $C_{L_{max}}$, the stall speeds of the aircraft for clean and full deflection of the flap were calculated. The stall speed was 128km/hr for a clean airfoil, which is 26.7% higher than the design value. The stall speed for full deflection of flap is 108km/hr, which is 29.7% higher than the specified value. The difference was probably due to the fact that lift produced by the fuselage and the tail plane is overlooked in Equation [4], which may contribute to 10 - 12% of total lift produced by the aircraft.

Figure 13 gives the variation of the lift coefficient with the angle of attack for the aircraft. Interestingly, the curve shows three humps at α = 6°, 16° and 26° indicating that the aircraft experiences stall at three different angle of attacks.

CONCLUSIONS

The wind tunnel tests show that the models of the canard and the wing of Eagle aircraft 150 have good aerodynamic characteristics. The maximum lift coefficient for canard (clean) is 1.32 and for the wing (clean) is 0.96. The slotted flap at full deflection angle of 35° increases the lift coefficient by 31.25% for the wing and 50% for the canard, as compared to the clean flap. The stall speed calculated on the basis of experimental values of lift, is higher than the designed value. This is because in the present calculations, the lift contributed by fuselage and tail plane has not been considered which contributes to about 10 - 15% of the total lift produced by the aircraft. The overall aerodynamic performance of the aircraft shows that the aircraft stalls at three different angle of attacks as the angle is increased. For a canard position with vertical offset, like in the aircraft understudy, different locations of the canard wake and leading edge vortex can significantly change the canard-wing flowfield and hence affects the overall aerodynamic performance of the aircraft. Further investigation is to be carried out to establish the understanding of the disturbed flowfield and the interference aerodynamics for this dual-wing aircraft.

FUTURE WORK

The results discussed in this paper are part of a larger study on the flow interaction between canard and wing using CFD and flow visualization techniques. Further investigations will also be carried out on larger size models in a large and high-speed wind tunnel using LDA.

ACKNOWLEDGEMENT

The study being conducted is supported by the IRPA long-term research grant offered by the Ministry of Science and Technology Malaysia. The authors also wish to thank Mr. George Blower, Chief Operating Officer, CTRM and Mr. Tim Burton, Chief Designer, Eagle Aircraft, Australia, who made available technical specifications of the aircraft and also for their support and thought provoking discussions.

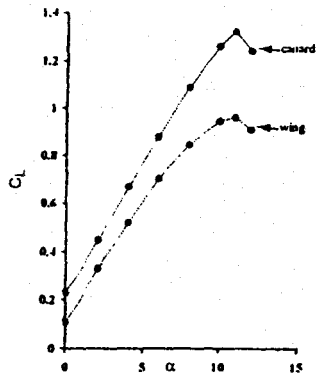

Figure 6 : Coefficient of Lift vs. Angle of Attack (Zero Flap Deflection Angle)

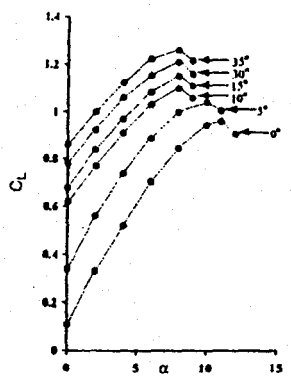

Figure 7 : Wing - Coefficient of Lift vs. Angle of Attack

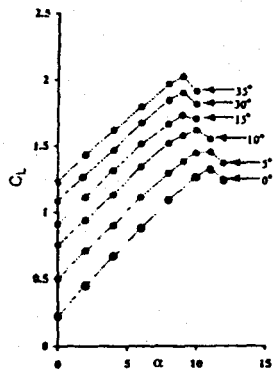

Figure 8 : Canard - Coefficient of Lift vs. Angle of Attack

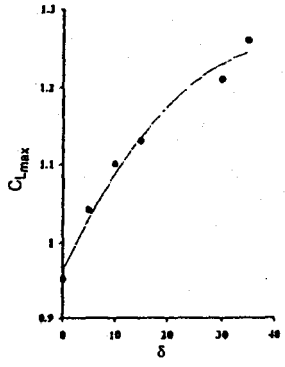

Figure 9 : Wing - Maximum Lift Coefficient vs. Flap Deflection Angle

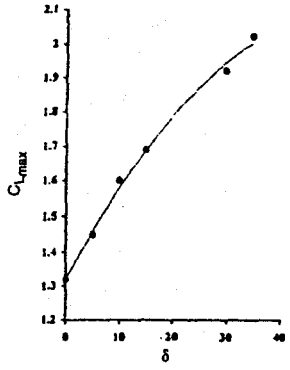

Figure 10 : Canard - Maximum Lift Coefficient vs. Flap Deflection Angle

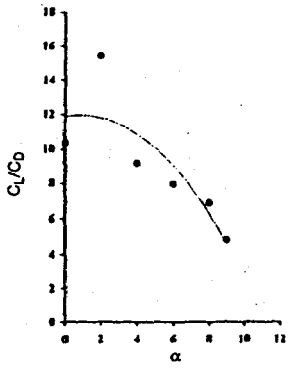

Figure 11 : Wing - Ratio C_L/C_D vs. Angle of Attack (Flap Deflection = 10%)

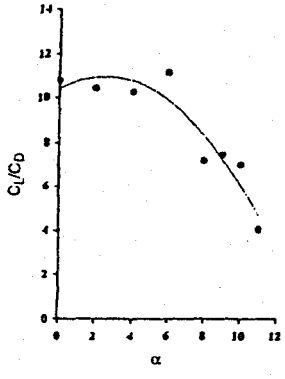

Figure 12 : Canard - Ratio C_L/C_D vs. Angle of Attack (Flap Deflection = 10%)

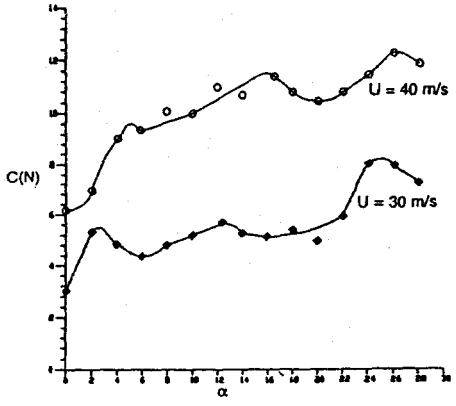

Figure 13 : Lift vs. Angle of Attack of the Model Aircraft

REFERENCES

Abbot I.H., Doenhoff E.V., 1959, Theory of Wing Sections, Dover Publications., NY.

Bottomley, J., 1977, Tandem Wing Aircraft, Aerospace (UK), Vol. 4, October 1977, pp. 12-20

Calarese, W., 1984, Close-Coupled Canard Wing Vortex Interaction, J Aircraft, Vol. 21, No. 2, February 1984

Horney, D.J., Fanjoy, D. W., 1997, A Study of Tandem-Airfoil Interaction in Different Flight Regimes, AIAA Paper 97-0515

Hoffmann, J. A., 1991, Effects of Freestream Turbulence on the Performance Characteristics of an Airfoil, AIAA Journal, Vol. 29, No. 9, September 1991

McGeer, T., Kroo, 1., 1983, A Fundamental Comparison of Canard and Conventional Aircraft, Journal of Aircraft, November 1983

Tu, E.L., 1992, Effect of Canard Position on the Longitudinal Aerodynamic Characteristics of a Close-Coupled CanardWing-Body Configuration, AIAA Paper 924632

CFD SIMULATION AND AERODYNAMICS OF LOW SPEED TANDEM WING DESIGN AIRCRAFT

Z.Husain, M.Z.Abdullah and T.C.Yap

School of Mechanical Engineering
Engineering Campus
University Science Malaysia
Nibong Tebang, Pulau Pinang

ABSTRACT

CFD results on canard and wing aerofoils of tandem wing design aircraft is validated by the wind tunnel tests. The experiments carried out in low speed open circuit wind tunnel at Reynold's number 2.25×10^5. The lift and drag coefficients are determined by varying the angle of attack from 0-16°. Use of flaps to full deflection of 35 deg.increases the lift coefficient of aerofoil wing and canard to 37.5% and 55% respectively. At all flap deflections canard and the wing stall at lower values of angle of attack compared to clean airfoils. A typical lift curve shows that it is smooth, gradual, a typical characteristic of this aircraft. The experiments also carried out on a aircraft model of scale 1:25, comparatively small for wind tunnel tests. The flow interaction between canard and wing was studied and verified by flow visualization technique. CFD simulation results using Fluent 5.5 were validated with the wind tunnel results.

Keywords : Canard, Wing, Tandem wing, Lift coefficient, Angle of attack.

INTRODUCTION

Potential of dual wing aircraft configuration has been realized for almost 75 years Bottomley (1977). The aircraft can have up to 50% reduction in induced drag due to distribution of the lift between the two wings apart from structural and weight benefits. The presence of canard as front wing provides rapid pitch control and the aircraft can immediately recover from stalling by creating negative pitching moment when stall happens provided the center of gravity is located between the two wings.

Theoretical research conducted by McGeer e tal (1983) has suggested that tandem wing configuration can be optimized better than conventional configurations under all flight conditions. Proper utilization of canard, however, requires understanding of the influence of canard on the flow behavior over the main wing. Two dimensional (2-D) airflow has been the subject of research for the past decades because of special interest on the structure and dynamics of airflow wakes as a function of Reynold's number. In contrast to single airfoils there is comparatively little information on the flow between airfoils in tandem arrangement. Calaverse (1984) studied close-coupled canard-wing vortex interaction.

The tests were performed at low Mach no. at various degrees of angle of attack. Three configurations were studied namely (i)coplanar (ii)canard placed higher than wing (iii)without canard. The results show that the leading edge of sweptback wings at moderate and high angles of attack separates and produces vortex sheets that roll up into vortices on the wings upper surface. When canards are closely coupled with the wings an interference between leading edge vortices occurs. The interference changes the turbulence characteristics and trajectories of the vortices. Tu (1992) concluded that the proper positioning of canards is essential to optimize aerodynamic performance as well as desirable stability and control characteristics. Most of the investigators concentrated on aerodynamics of tandem swept or delta wings in higher speed regime. Fanjoy (1997) investigated tandem wing in transonic range. The results show that at positive angles of attack, the lift/drag ratio of leading aerofoil is increased and trailing airfoil eperiences less lift and drag due to reduced local angle of attack. The paper is short of obtaining the best stagger distance. Sigal (1999) made studies on modular model consisting of cruciform canard mounted on a thin forebody and five interchangeable thick main bodies behind it. The study included the canard flow interaction with the ever increasing diameter bodies on lateral position of trailing canard vortices. Apart from studies on tandem aerofoil studies conducted on tandem arranged bluff bodies, Luo (1990) reports the measurement of aerodynamic forces on a square cylinder which was downstream to identical cylinder. The study made by changing the position of downstream cylinder in x and y direction. The investigations showed that for tandem formation (y/D =0) a critical spacinon is formed to exist at L/D ~ 4 in this range of L/D downstream cylinder is subjected to thrust. For spacing larger than critical value reattachment does not take place and both cylinders shed vortices and both are subjected to drag forces. For staggered formation Y/D ± 0 the lift forces on downstream cylinder deviates from zero at certain positions of L/D and Y/D.

EXPERIMENTAL DETAILS

All the experiments were carried out in open loop wind tunnel (Figure 1) at the School of Mechanical Engineering, University Sains Malaysia. The working section of the wind tunnel is 600 mm long and has 300 mm(H) and 300 mm(W) cross-section. The experiments conducted at maximum wind tunnel speed of 38 m/s at such a speed the turbulence intensity of flow was 2.5%. The two airfoils were made from fiber glass. The experiments conducted on rectangular plan form airfoil section of canard with span of 292 mm, chord 92 mm in semi-span aspect ratio of 6.4 and wing span of 292 mm, chord 62 mm in semi-span aspect ratio of 9.4. The wind blockage based on width of largest airfoil was 30 %. Based on the characteristic dimension as chord of the airfoil the flow Reynolds number of canard was 2.25×10^5 and wing 1.5×10^5 respectively. The wind tunnel is provided with three component electronic balances for the measurement of lift, drag, turning moment, and seven channel data acquisition system to record and display the pressure, relative humidity, velocity, temperature, lift, drag and turning moment on the computer monitor. The airfoil made from fiber was joined at both ends with aluminum plates resulting in box-shaped (bi-wing) assembly. One of the plates is screwed to a steel rod connected to the electronic balance. The whole assembly can be rotated through 360 deg. permitting any degree of angle of attack with respect to airflow.

RESULTS AND DISCUSSION

In literature survey one does not find any aerodynamics study carried out on canard and wing separately. The canard-wing configuration is considered as one unit and the forces acting on them and the interaction of fluid flow being considered. In the present study wind tunnel experiments on canard and wing was carried out with the same aspect ratio as aircraft wings and maintaining geometric similarity.

Figure 2 shows relation between coefficient of lift and angle of attack for the canard and the wing. The coefficient of lift, C_L varies with angle of attack, α and increases up to stall. The stall angle for both airfoils is 11 deg. The value of C_L is greater for canard than wing for all values of α. The maximum value of C_L for canard is 1.32 and for wing it is 0.96.Figure 3 shows relation between coefficient of lift and angle of attack at various values of flap deflection (δ). The flap deflection is varied from 0-35 deg. At full deflection percentage increase in coefficient of lift for

the canard is 50 % and for the wing it is 31.5 %. The maximum lift coefficient at stall increases with flap deflection whereas the stall angle itself decreases. The flap deflection changes the geometry of the camber line and results in increase in lift. Figure 4 gives relation between ratio of C_L/C_D (performance efficiency of the airfoil) with angle of attack. The best value of C_L/C_D=10 is obtained at zero angle of attack, $\alpha = 0$ and it decreases with increase in α.

The canard–wing configuration based on geometric similarity between prototype and the model is shown in Fig (5). In the investigation the horizontal distance between the two airfoils was kept constant and the wing position changed vertically from tandem position (Z/C=0) to staggered position (Z/C $\neq$ 0) as shown in Fig (6). The variation of coefficient of lift with α for various positions of the wing (0-0,0-1,0-2) is shown in Fig (7). The objective was to obtain the optimum position for the wing.

The arrangements have also an effect on flow field between airfoils. The unfavorable lift and drag characteristics noted for low-wing configuration (0-1) was evident as angle of lift is increased. The configuration has maximum lift at position 0-2 which is the present location of the wing in the aircraft. Also to be noted discontinuity between 6-8 deg. of angle of attack. The readings could not be taken due to severe vibrations set up in the airfoil. The model aircraft made to a scale of 1:25 tested in the wind tunnel varying the angle of attack. Fig (8) shows relation between lift and at wind tunnel speed of 30 and 40 m/s. The interesting part is gradually increasing lift with angle of attack The curve has three humps at angles 6, 16 and 26 deg.which means that the aircraft experiences stall at these points. The lift falls for a short period at these points.

Smoke flow experiments were conducted at a reduced velocity of 10 m/s. Smoke is generated by heating electrically shell ondina oil inside a probe. The probe is held at inlet of the test section and the generated smoke flows over the models in the test section. Fig (9) shows the assembly of canard-wing configuration in position (Z/C =0.22).In the figure clearly visible highly turbulent flow at the inlet edge of the wing. Fig (10)shows the aircraft model at an angle of attack of zero degrees .The streamlined flow behind the hump is clearly visible.

CFD SIMULATION

In recent years studies have been carried out including methods of predicting lift and drag as well as aerodynamic performance and considerable progress has been made in this direction. For two-dimensional airfoils with and without flaps numerical calculation methods based on potential theory are now available. Computational

Fluid Dynamics (CFD)code 5.5 has been used to investigate the aerodynamics of Eagle aircraft wings. The canard and wing airfoils investigated with chord of 92 mm for canard and 62 mm for the wing. The models were mesh in GAMBIT using pave type unstructured mesh.(GAMBIT is a software package designed to help analysts and designers build and mesh models for CFD and other scientific applications).The angle of attack of both airfoils varied from 0-14 deg. and the flap deflection from 0-35 deg. The lift and drag coefficients obtained from simulation are compared with wind tunnel results. Besides this velocity profile, pressure contour, and turbulent kinetic energy vector of the airfoils presented. The Reynolds stress model was used in simulation as turbulent model. The inlet boundary condition were set at 38/s ,kinetic energy as $1.237 m^2/s^2$.and turbulent intensity as 2.4 %.The air density ,viscosity set for ambient temperature of 300 K. For the analysis the under relaxation factors were set as default shown in Table I

TABLE 1 : The under relaxation factors for simulation

Pressure	Momentum	Viscosity	Density	Body forces	Turbulent kinetic energy	Dissipation rate
0.3	0.7	1.0	1.0	1.0	0.8	0.8

The convergence criteria for all the equations which includes x-velocity, y-velocity, k, epsilon, uu stress, vv-stress ww-stress were reduced to 10^{-5}in order to get better results. Fig (11)shows CFD results for velocity vectors, velocity contours, pressure coefficient and turbulent kinetic energy for angle of attack and flap deflection zero. Fig (12) gives velocity vectors and turbulent kinetic energy for angle of attack equal to 12 deg. and flap deflection zero. Fig (13) gives velocity vectors and turbulent kinetic energy at angle of attack 10° and flap deflection 35°. Figure 14 gives the relation between CL and angle of attack by CFD technique for the canard.

CONCLUSION

NACA airfoils are generally used in aircrafts and their aerodynamic characteristics are available in literature. The Eagle aircraft wings are tailored made and had never seen the wind tunnel before. The wind tunnel tests has shown good aerodynamic characteristics. Full deflection of the flaps increases the lift coefficient of the wing by

about 50 % and canard by 31.5 %Wind tunnel and smoke tests showed that the wing occupies the optimum position with respect to canard.

The lift coefficient obtained by simulation is higher for canard than obtained experimentally as the losses has not been considered. The simulation technique is based on using steady state equations whereas separated flow behind the airfoils can become transient and not fully turbulent as assumed by Reynolds stress model.

ACKNOWLEDGEMENT

The authors like to thank the Malaysian Ministry of Science Technology &Environment for sponsoring this work under IRPA long term grant. The authors wish to thank Mr.George Blower, Chief Operating Officer, CTRM and Mr.Tim Burton, Chief Designer, Excelnet who made available to us the technical specifications of the aircraft and also for their support and thought provoking discussions.

FUTURE WORK

The studies presented in this paper are preliminary investigations on small scale models because of the constraints on the wind tunnel size. The tests must be conducted on large size models and on large size wind tunnels to give high Reynolds number for better evaluation of the results.

REFERENCES

Bottomley ,J. 1977. Tandem wing aircraft, Aerospace (U.K.), 14, pp 12-20

Calarese,W. 1984. Close-coupled canard-wing vortex interaction, Journal of Aircraft, 2(2).

McGeer, T.Kroo I. 1984. A fundamental comparison of canard and conventional aircraft Journal of Aircraft.

Tu, E.L. 1992. Effect of canard position on longitudinal aerodynamic characteristics of close-coupled canard–wing body configuration, AIAA 92-4632.

Fanjoy, D.Dorney, D.J. 1997. A study of tandem-airfoil interaction in different regimes AIAA 97-0515

Sigal A. 1999, The interaction between canard and thick bodies. Part II Analysis of Interactions AIAA- 99-3146

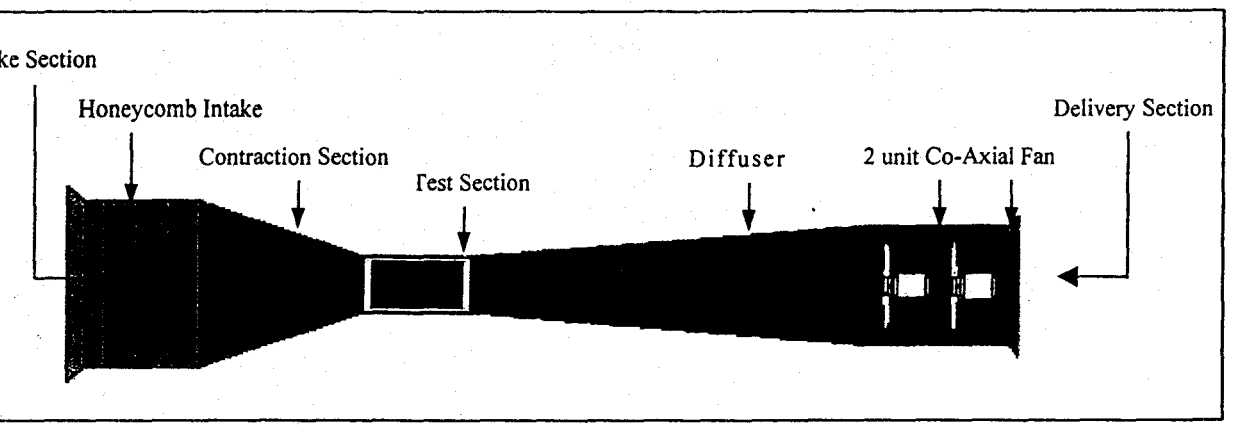

Figure 1: Open Circuit Wind Tunnel, USM

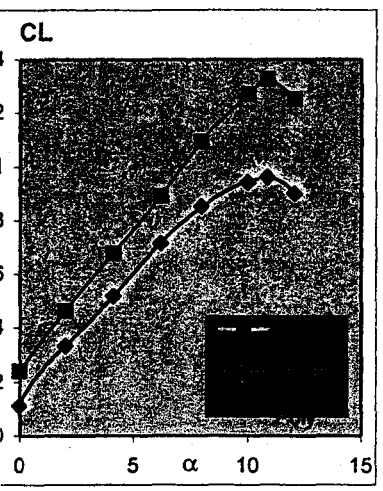

igure 2: Coefficient of Lift vs angle of attack

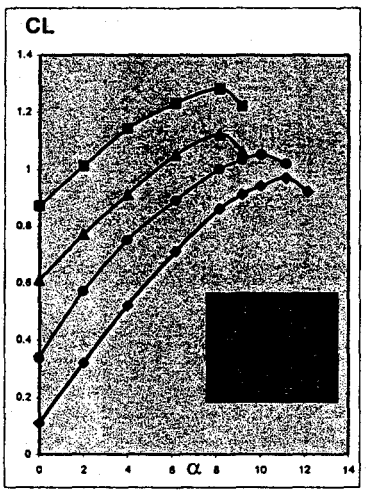

(a)

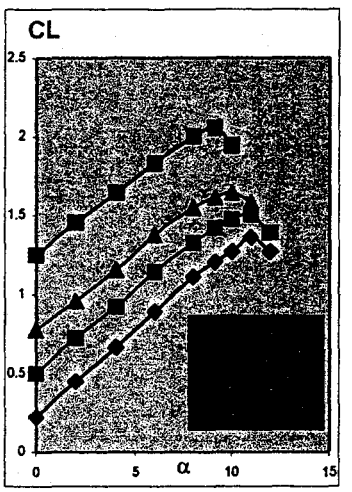

(b)

Figure 3:coefficient of lift vs angle of attack with various flap deflection. (a) wing (b) canard

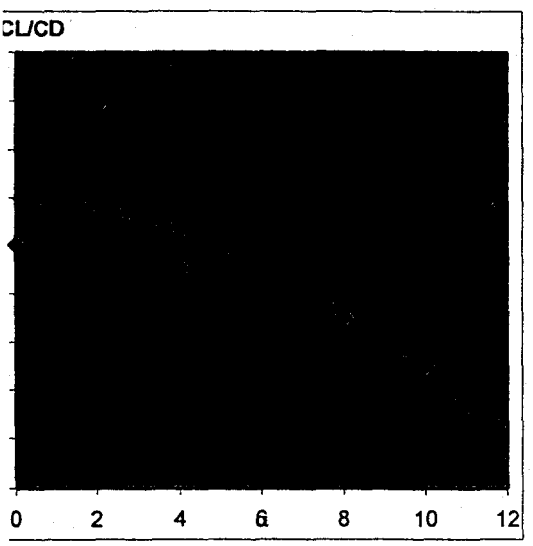

(a)

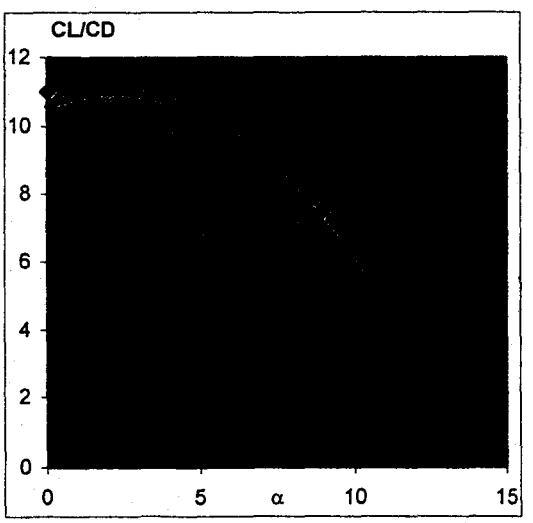

(b)

Figure 4: Ratio of C_L/C_D vs angle of attack (a) wing (b) Canard

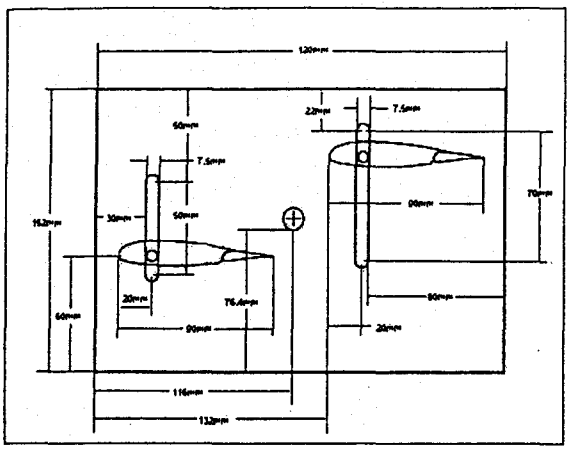

Figure 5: canard-wing configuration

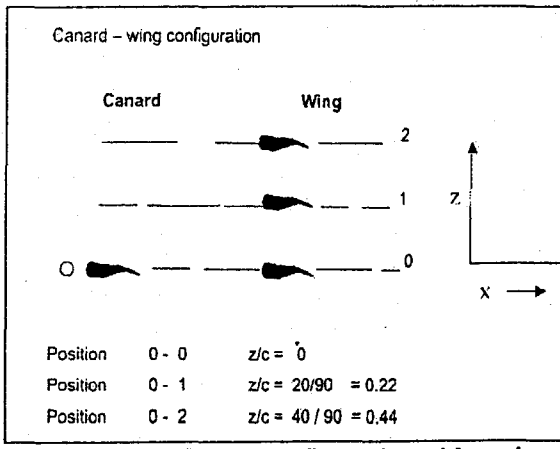

Figure 6: canard-wing configuration with various position of wing with respect to canard.

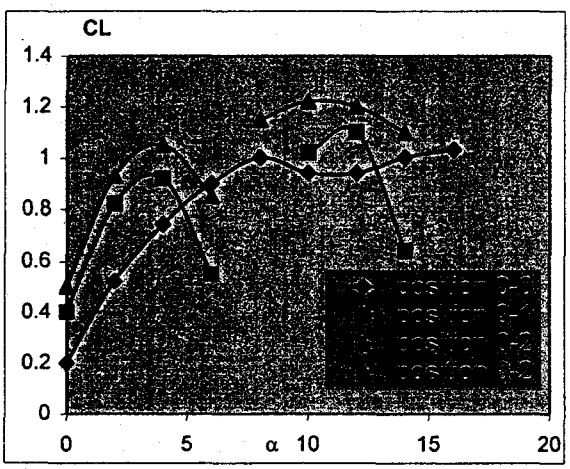

Figure 7: Graphs between coefficient of lift and angle of attack at various positions of wings: 0-0, 0-1, 0-2.

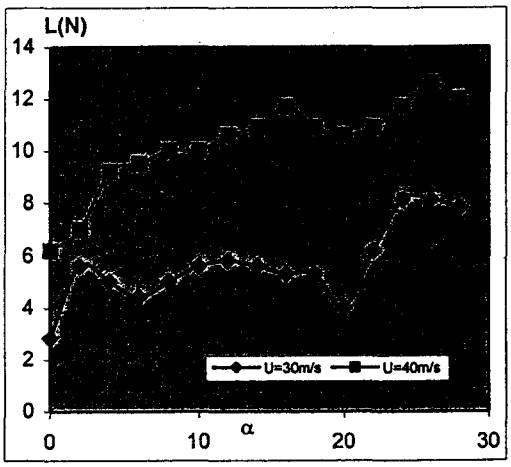

Fig 8: lift vs angle of attack for the model aircraft at 2 speeds.

Fig 9: Canard-wing configuration clearly visible turbulent flow at the leading edge of the wing in position z/c=0.22.

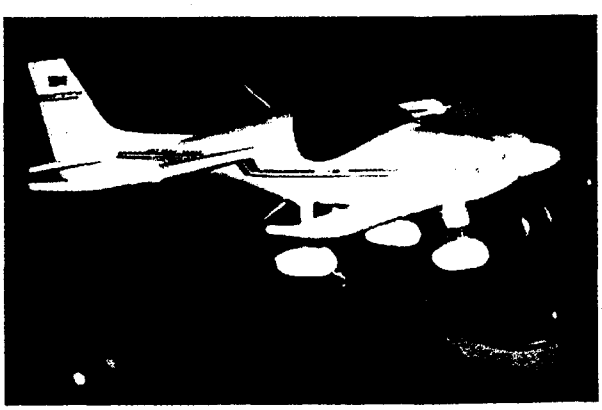

Fig 10: Shows a model of Eagle Aircraft clearly visible streamline flow behind the hump of the model.

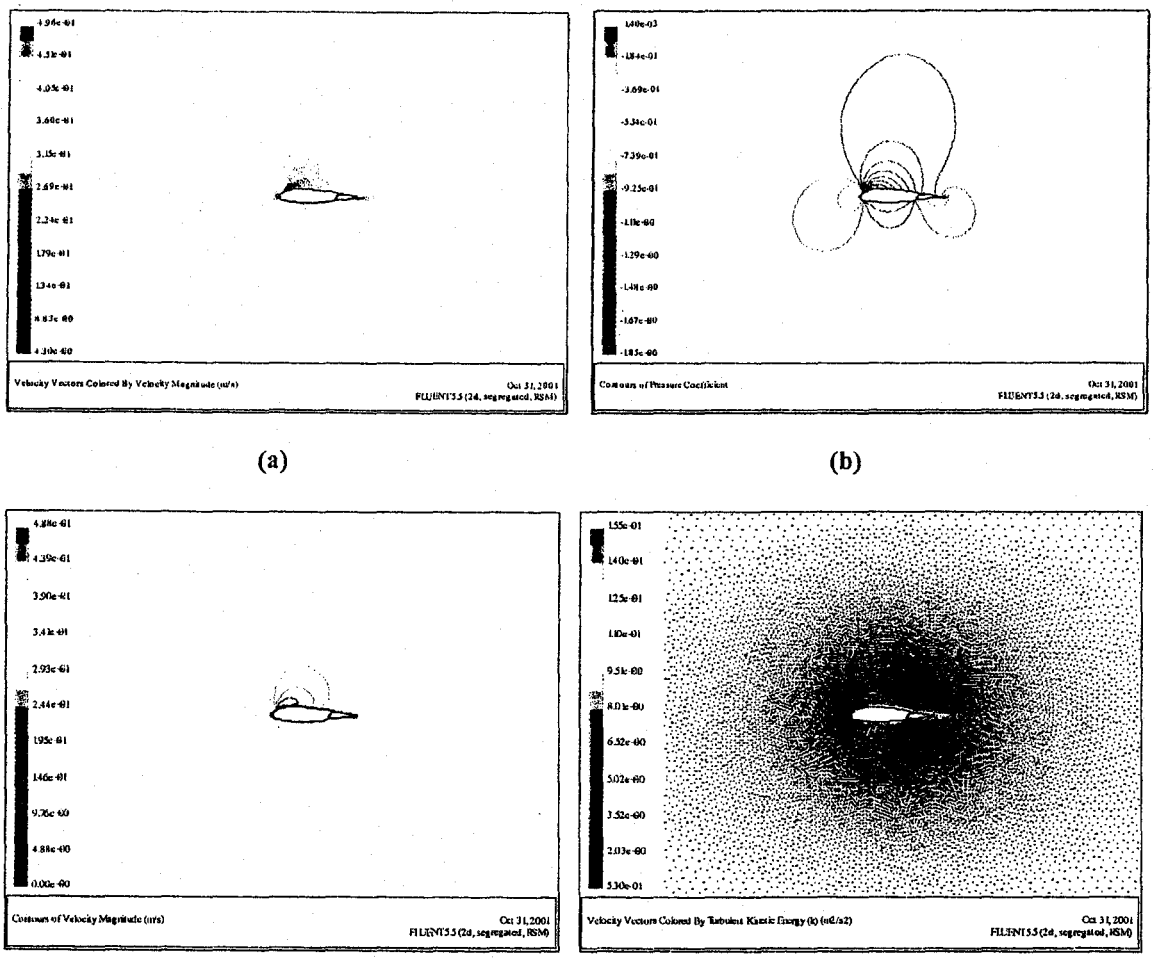

(a) (b)

(c) (d)

Figure 11: CFD simulation $\alpha=0$; $\delta=0$
(a) velocities vectors (b) coefficient of pressure (c) velocity contours (d) turbulent kinetic energy

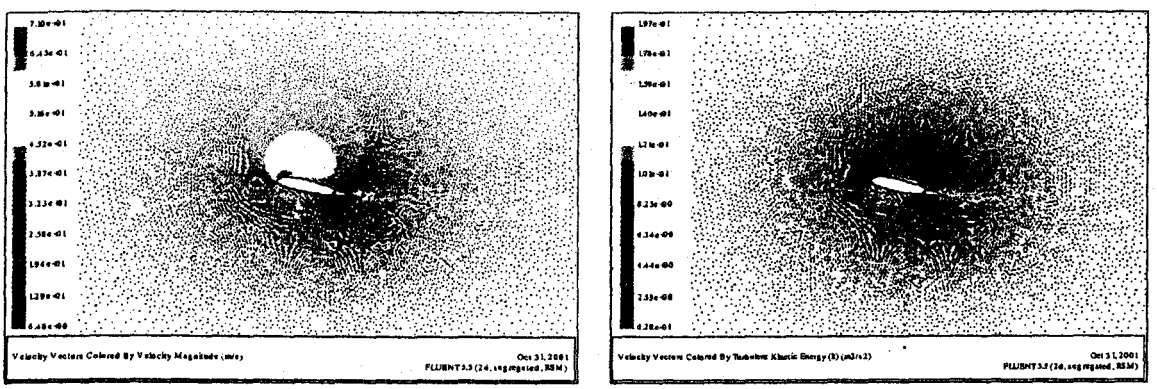

(a) (b)

Figure 12: CFD simulation; α=12°, δ=0°
(a) Velocity Vectors (b) Turbulent Kinetic Energy

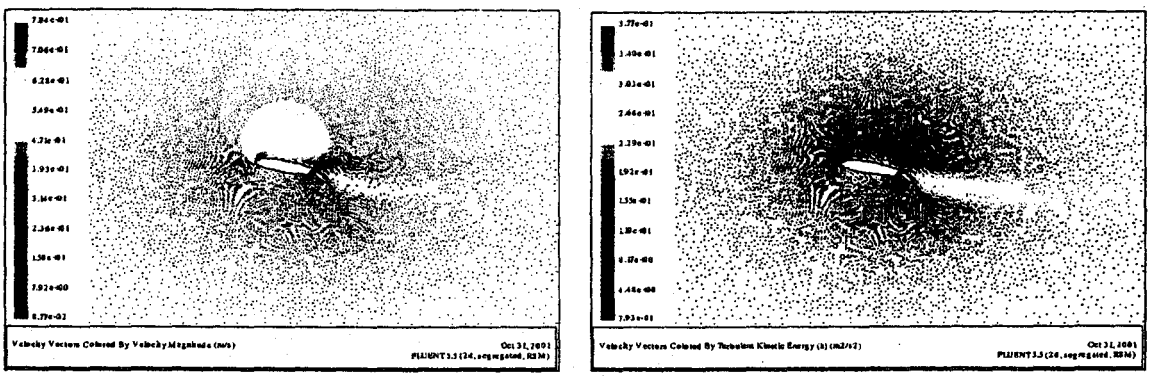

(a) (b)

Figure 13: CFD simulation; α=10°, δ=35°
(a) Velocity Vectors (b) Turbulent Kinetic Energy

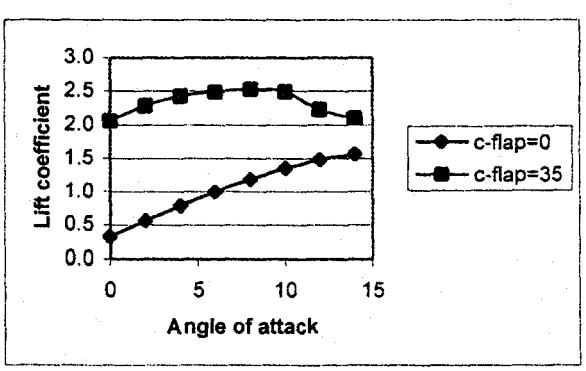

Figure 14: Coefficient of lift vs angle of attack using CFD simulation.

ANALYSIS OF FLOW INDUCED VIBRATION

Zaidi Mohd Ripin and S.L.Chong
School of Mechanical Engineering
Universiti Sains Malaysia
Engineering Campus
14300 Nibong Tebal
Seberang Perai Selatan
Tel: 04-5937788 ext 6302
Fax: 04-5941025

Keywords: cylinder; drag force; Strouhal number; vibration; wind induced

ABSTRACT

An object when put into a moving fluid will develop pressure field around its periphery which when integrated over the area resulted in the force, which is usually described as the drag force acting on the body in the direction of the fluid and the lift force acting on the direction normal to the free-flow stream. If the object is elastic enough there will be a motion, which will alter the pressure distribution around the surface and resulted in different force acting on the object compared to the previous one. This time-varying pressure distribution on the object and the resulting motion within the fluid flow is the objective of this research. The research begin with the study of a relatively simple one degree of freedom model where it is subjected to time-varying force associated with either the displacement or the velocity or the acceleration of the object based on the finding by other researchers. However the implementation of such forces (either linear or non-linear) do not result in a satisfactory outcome. Comparatively the best method comes from the drag force made as a function of time sinusoidally varying according to the Strouhal frequency. The results obtained are comparable with that of other published results. The work then extends to include the analysis of pressure distribution around a cylinder for unsteady flow using MATLAB based CFD-FEM model and the drag forces determined over time for static and moving cylinder. The initial results showed that the approach is able to predict the time varying drag forces and the vortex frequency does not vary much for static and moving cylinder.

INTRODUCTION

Fluid structure interaction occurs in many engineering field. These interactions give rise to complicated vibration of the structure and could cause structural damage under certain unfavorable condition. A common fluid structure interaction problem is the flow-induced vibration on a structure caused by vortex shedding. Numerous experimental and numerical studies have been carried out on the fluid structure interaction problem (Zhou 1999). Early experiment concentrated on rigid structure in a cross flow. Later investigations dealt with elastic structure because of their importance in many engineering fields. In spite of these later studies, the investigations of fluid- structure interaction are far from complete (Zhou 1999).

The prediction of flow induced vibration is currently based on semi-empirical methods, often employing a 'strip theory' approach and relying on experimental data base, which are often obtained through a number of simplifying assumption (Hover 1997). In this paper some obvious fluid phenomena when laminar flow passing through circular cylinder such as vortex action behind the cylinder, the change of the relative velocity between the fluid and the cylinder and the changing of drag coefficient are used as the force input to system.

If a circular cylinder is placed in a uniform stream, then a periodic, asymmetric distribution of vortices is generated in the wake for Reynolds number between 50 and 3×10^5 (Griffin 1972). Vortex is shed alternately from the upper and lower surfaces of the cylinder at constant frequency. The alternate shedding of vortex causes oscillating streamline in the wake, which in turn leads to an oscillating pressure distribution. The oscillating pressure in turn gives rise to oscillating drag force at twice strouhal frequency acting normal to the cylinder (So 2000).

When the cylinder is in static condition, the drag force acting on it is a function of free stream velocity of fluid. If after the action of the force on the cylinder, the cylinder starts moving, the drag force becomes a function of relative velocity of fluid and cylinder.

According to Zhou (1999), when the flow passes through the cylinder, a flow equal and opposite to that of the cylinder response is superimposed to the flow field due to the reference frame fixed with cylinder. The flow is then solved subject to this additional velocity. Consequently, an additional is added to the drag coefficient related to the acceleration of the cylinder. The effect of the fluid phenomena mention above toward the system response will be studied.

METHODOLOGY

Analysis of flow-induced vibration in this case is carried out by modeling a cantilever in a flow field. The cylinder is modeled as simple damped mass-spring system The equivalent stiffness value for the first bending mode considerd, K_{eq}= (3EI)/L The damping constant as determine from experiment is about 2% of critical damping value. The mass of cylinder is 6.65g and the stiffness value is 253.4112 N/m and the damping value is 0.0519 N/ms^{-1}.

From the literature review there are three main excitation mechanisms for wind-induced vibration that can be used:

i) the change of relative velocity with wind over the cylinder as it acquire motion,

$$F(t) = 0.5\, C_d \rho A(U-\dot{x})^2 \quad \text{.....(1)}$$

ii) the alteration of C_d due to acceleration of the cylinder, $C_d^* = C_d + \frac{\pi D}{2U^2}\ddot{x}$ and the altered C_d can be used in the forcing function as: (Zhou, 1999)

$$F(t) = 0.5\rho AU^2\left(C_d + \frac{\pi D}{2U^2}\ddot{x}\right) \quad \text{.....(2)}$$

iii) pressure fluctuation at twice Strouhal frequency, (So,2000)

$$F(t) = 0.5C_d\rho AU^2 \sin 2\omega t \quad \text{.....(3)}$$

Based on the above, a cylinder in a flow field will be subjected to the forces arising from the fluid structure interaction. The equation of motion of a cylinder can then be represented by:

$$M\ddot{x} + C\dot{x} + Kx = F(t)$$

The effect of the F(t) from three main mechanism listed above will be investigated. Solution of the time response for forcing function (i) and (ii) are obtained from Runge-Kutta fourth order method and case (iii) is solved using Newmark method. The time response of the system to each excitation mechanism is then plotted. However it is a known fact that the mechanisms above are empirically determined. It is of major interest to the authors to investigate how the unsteady flow modeling can be used to determine the pressure fluctuations due to vortex shedding behind the body in order to establish the forcing function.

MATLAB software is used for solution based on computation fluid dynamic using finite element method to determine the pressure distribution around a cylinder due to unsteady flow. In this analysis, there are four components to be considered. Figure 1 shows the overall method used in the flow-induced vibration. The first is flow analysis. As the flow passes the static cylinder, velocity distribution over cylinder and the drag force frequency will be investigated. The second is the calculation of structural dynamic. The third is the fluid-structure interaction. The effect of the structure motion toward fluid flow

will be taken into consideration. Finally is mesh remapping for structural analysis..

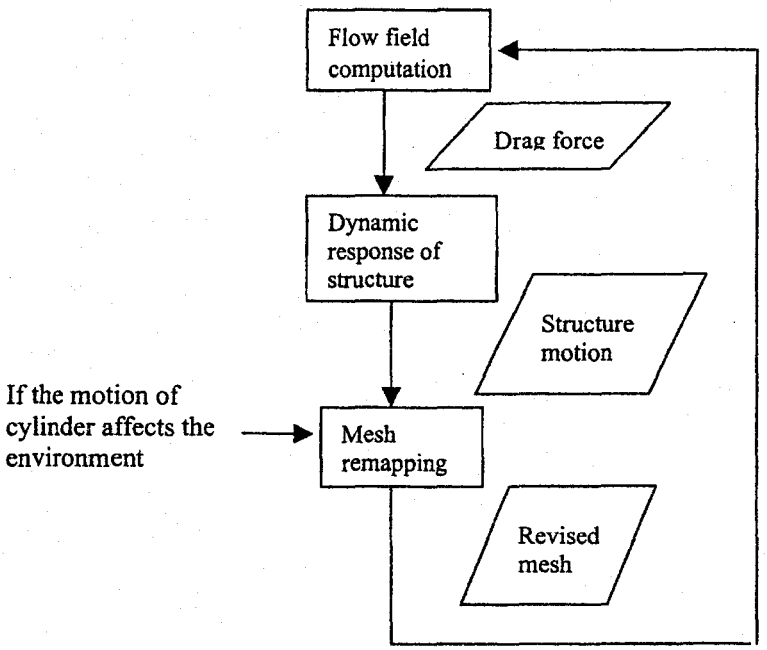

FIGURE 1: Flow chart illustrating flow induced vibration methodology

RESULTS AND DISCUSSION

Figure 2 shows the response of the single degree system with forcing function (1). The graph shows that the cylinder will be displaced from zero to an initially high deflection and will oscillate at a frequency of 32.5 Hz with the oscillating dying out to a steady state position. The damping from the response curve is equal to 0.0243 N/ms^{-1}. The relative velocity between the wind velocity and the system velocity does not contribute to the steady state vibration of the system.

Figure 3 shows the response of the single degree system with forcing function (2). This forcing function is only responsible for the transient vibrating response at the beginning and pushes the system to a new equilibrium position. The new

equilibrium position is equal to the displacement of spring with equal stiffness value when drag force, $F(t) = 0.5C_d\rho A(U)^2$ applied. Figure 2 and 3 showed almost similar results. Both figures indicated the same new equilibrium position

Figure 4 represent the response of the system when the forcing function (3) is applied. The system vibrates at equilibrium position of zero and frequency of vibration is equal to twice Strouhal frequency.

Figure 5 shows the amplitude response for alternate vortex shedding using forcing function (3). The amplitude of vibration at steady state condition is calculated at different reduced velocity, V_r. The trend shown in the figure is similar to the measurement by Wooton and the calculation using Van Der Pol model (Turnbull 1984). The maximum amplitude occurs at reduced velocity of about 2.5. This is due to resonant accuring at reduced velocity of 2.5. The difference in maximum amplitude value is due to the different damping value applied in each case

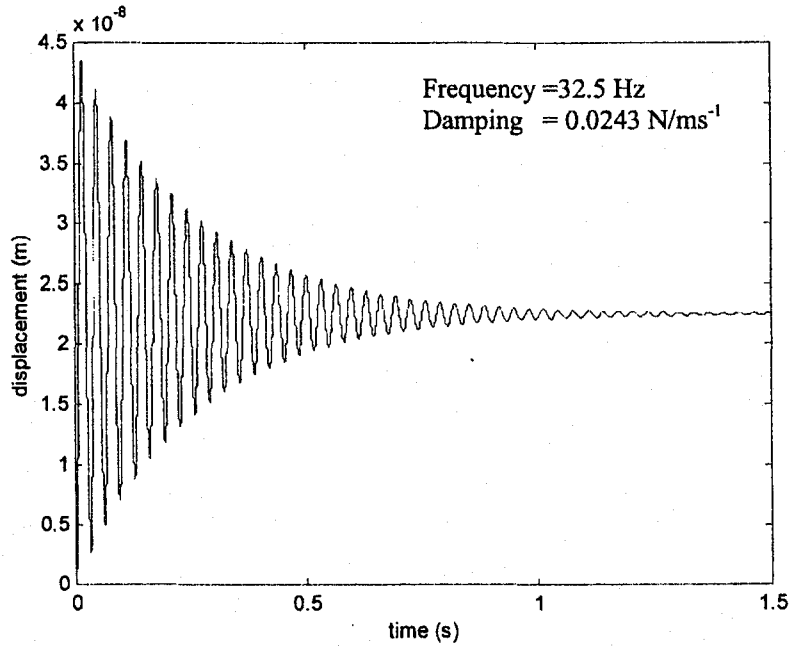

FIGURE 2: Response of the system with forcing function as a function of system velocity

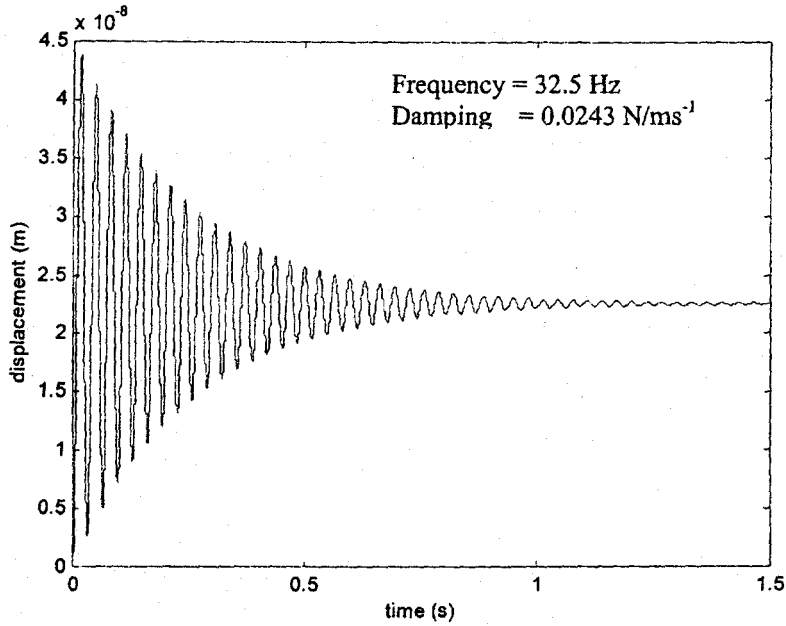

FIGURE 3: Response of the system with forcing function as a function of system acceleration

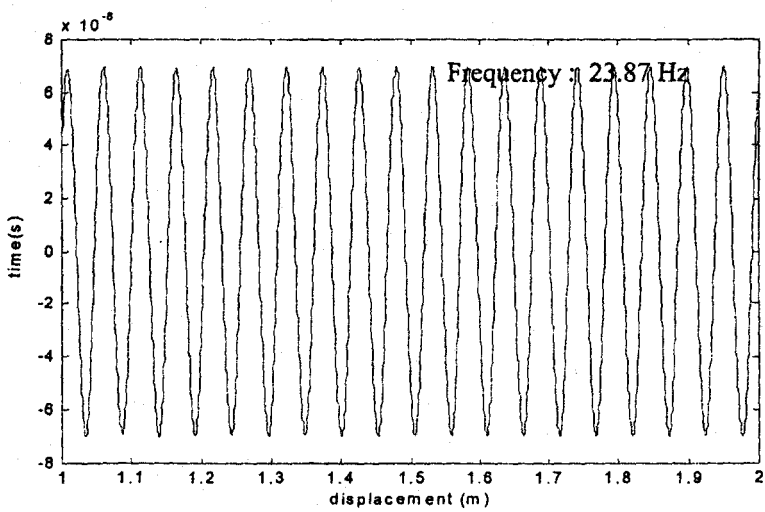

FIGURE 4: Response of the system with forcing function as a function of Strouhal frequency

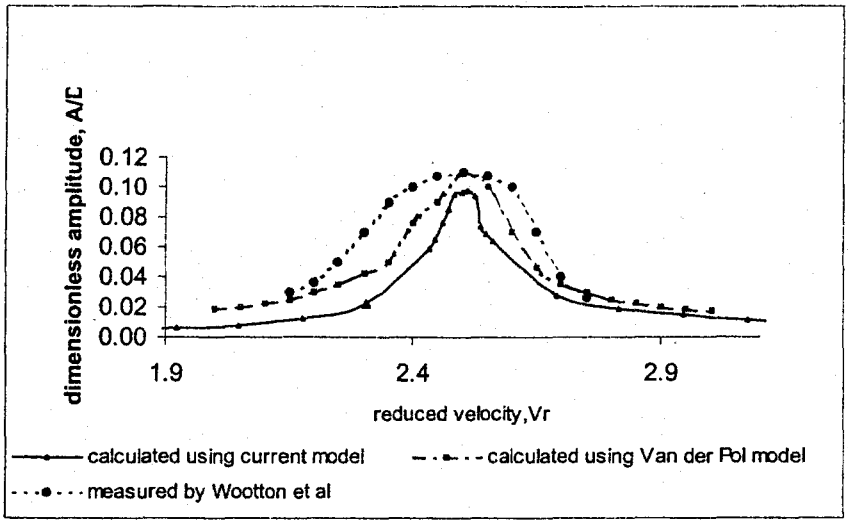

FIGURE 5: Amplitude response for alternate vortex shedding

COMPUTATIONAL FLUID DYNAMIC ANALYSIS OF UNSTEADY FLOW

The computer simulation of the flow around cylinder is done using FEMLAB (Comsol, 2000). The model is used to represent the flow around a cylinder in a wind tunnel.The drag force acting toward the cylinder is calculated by integrating the pressure distribution around the cylinder surface. Figure 6 shows the meshing used in the analysis.

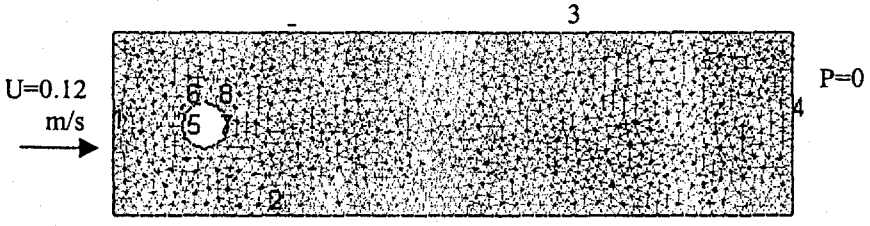

Figure 6: The meshing used in the unsteady flow analysis

The incompressible Navier-Stokes equation is given as below:

$$\frac{\partial \mathbf{u}}{\partial t} = -\nabla \Pi + \mathbf{u} \times \boldsymbol{\Omega} + \nu \nabla^2 \mathbf{u} ,$$

where $\Pi = p/\rho + \mathbf{u} \cdot \mathbf{u}/2$ and $\boldsymbol{\Omega} = \nabla \times \mathbf{u}$

The Navier-Stoke equations are solved together with incompressibility constraint $\nabla \cdot \mathbf{u} = 0$

The inflow velocity is applied at boundary 1 as shown in figure 6. For boundary 2,3,5,6,7 and 8 the no slip condition is applied implying static condition and zero pressure is assumed at boundary 4. Figure 7a shows the velocity distribution of flow around the cylinder at t = 45s, Reynolds number 800 and inlet velocity 0.12 m/s. The simulation of the flow around the cylinder start from 0 to 45 seconds with the time interval of 0.5 second. Figure 7 shows that the flow velocity does not distribute evenly along the surface of cylinder. The minimum velocity occurs behind cylinder. Alternate vortex formation behind cylinder resulting in unsteady drag force. The time history of drag force acting on the cylinder is determined by integrating the pressure distribution around the surface of the cylinder.

It is of interest to the authors to investigate the effect of constant velocity moving cylinder on to the velocity distribution and the drag force. A similar model was used as in figure 6 except the boundary conditions for surface 5,6,7and 8 are now changed to having velocity 0.2m/s to the right. The velocity distribution from the analysis at time 45 second is shown in figure 7b. The velocity also does not distribute evenly. The vortex start forming at distant far from the cylinder compare to static cylinder.

Figure 8 shows the time history of drag force for the stationary and the moving cylinders with same initial and boundary conditions. The drag force acting on both cylinders is a sinusoidal function with frequency is twice the Strouhal frequency. These results are comparable with what have been obtained by So (2000). The results showed that the frequency and the average value of drag force for stationary cylinder and moving cylinder do not vary much. The amplitude of fluctuation for both cylinders is different.

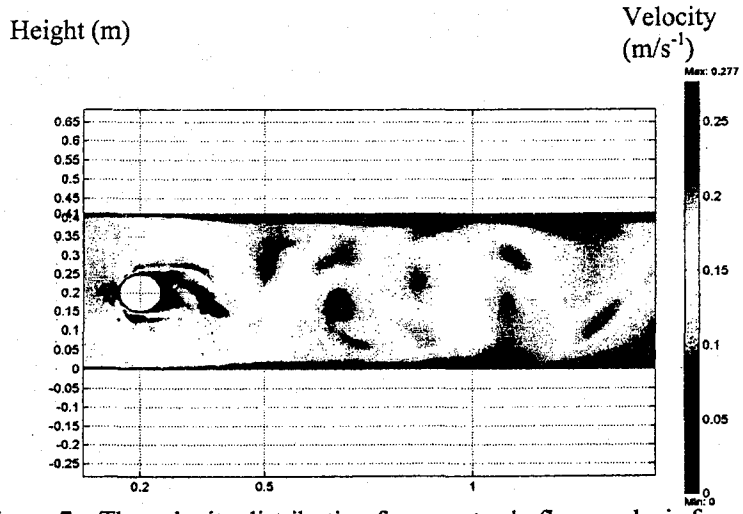

Figure 7a: The velocity distribution from unsteady flow analysis for static cylinder at Re = 800 and t=45s

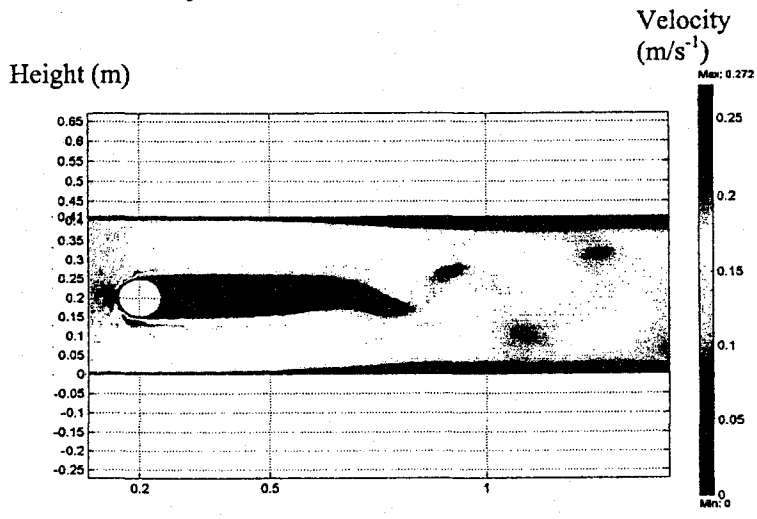

Figure 7b: The velocity distribution from unsteady flow for moving cylinder at similar speed and t=45

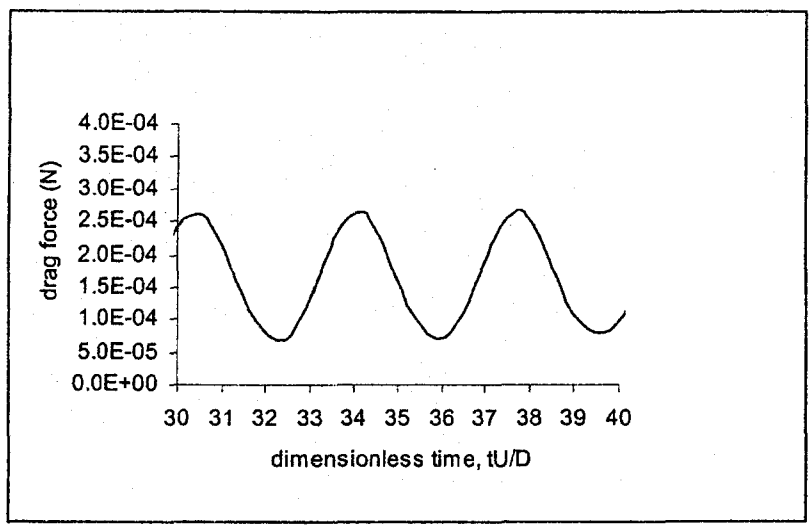

Figure 8a: Time history of drag force for stationary cylinder under unsteady flow

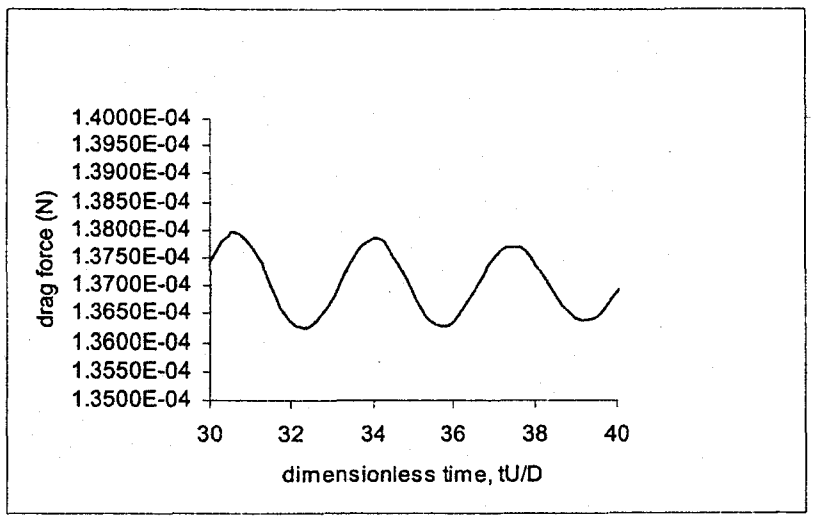

Figure 8b: Time history of drag force for moving cylinder under unsteady flow

CONCLUSION

For the three forcing function applied to the system only forcing function with Strouhal frequency contributes to the vibration of the system. The effect of other forcing function pushes the cylinder to a new static equilibrium position. After taking consideration of the effect of these three forcing function, it can be concluded that when uniform flow pass through a circular cylinder, the cylinder will move to a new equilibrium position and vibrate about that mean position. The simulation of flow around cylinder shows satisfactory result where unsteady flow develops behind the cylinder indicating alternate vortex formation. The effect is translated into varying pressure on the cylinder. Integrating the pressure component in the horizontal direction resulting in the drag force. The results indicated the force to vary at frequency twice of Strouhal frequency. The effect of moving the cylinder along the flow stream reduces the drag force, however the alternating frequency remains the same.

NOTATIONS

A	Amplitude of vibration	m
a	System acceleration	m/s^{-2}
C_d	Drag coefficient	
D	Diameter	m
E	Modulus of elasticity	N/m^2
f_n	Natural frequency of silinder	Hz
I	Momen inertia of area	m^4
L	Length of silinder	m
U	Free stream fluid velocity	m/s
u	Fluid velocity vector	m/s
V_r	Reduced velocity = $\frac{U}{f_n D}$	
x	Cylinder streamwise direction diplacement	m
ρ	Fluid density	kg/m^3
Ω	Fluid vorticity vector	m/s
ω	Strouhal frequency	rad/s

ACKNOWLEDGEMENTS

The authors wish to acknowledge support given by Ministry of Science, Technology and Environment through IRPA long-term grant account no. 06343

REFERENCES

Comsol,Inc.,2000, FEMLAB version 2.0 user's guide and introduction, USA: Comsol, Inc.

Griffin, O.M., 1972, Flow near self-excited and forced vibrating circular cylinders, *Journal of Engineering for industry,* 539-547.

Hover, F.S., Techet, A.H. & Triantafyllou, M.S., 1998, Forces on oscillating uniform and tapered cylinder in crossfow, *Journal of Fluid Mechanic* 363, 97-114.

Staubli, T., 1983, Calculation of the vibration of an elastically mounted cylinder using experimental data from forced oscillation, *Journal of fluids engineering* 105, 225-229.

So, R.M.C., Liu, Y., Chan, S.T. &Lam, K., 2000, Numerical studies of a freely vibrating cylinder in a cross-flow. *Journal of Fluid and Structures* 15,845-866.

Turnbull, D.H. & Currie, I.G., 1984, Flow-induced oscillation of cylinder in streamwise direction, *Symposium of flow-induced vibration* 1, 73-84.

Zhou, C. Y., So, R. M. C. & Lam, K., 1999, Vortex-Induced vibration of an elastic circular cylinder, *Journal of Fluid and Structure* 13, 165-189.

BUCKLING ANALYSIS OF COMPOSITE TUBES DUE TO EXTERNAL RADIAL IMPULSIVE LOADING.

Roslan Ahmad and Mohd Radzai Said
School of Mechanical Engineering, Engineering Campus,
Universiti Sains Malaysia, 14300 Nibong Tebal, Pulau Pinang, Malaysia

Keyword : buckling, carbon fibre reinforced plastic, finite element method

ABSTRACT

The finite element method is employed to examine the elastic buckling of 3 covers, with two plies per cover of (+5/-5°) fibre orientation of carbon fibre reinforced plastic cylindrical shell subjected to dynamic external pressure pulse. The pressure wave generated is transmitted through the water filled space confined by the outer surface of the tube specimen and two rigid end plugs. The finite element analysis and results obtained from experiments and a closed form solution [1] were compared.

INTRODUCTION

Current research on laminated plate and shell is widespread and covers material failure under static and dynamic loading, the latter being applied in the form of impulses and impacts to the structures. In all cases should the loading acquire and exceed a certain limiting value, a complex failure mode will set in which is dependent on parameters such as the anisotropy orientation (relative to the general layout of material plies), the nature of induced stresses in the composite (tensile-compressive-shear acting individually or in combinations), the average impulse intensity and the geometry of the impactor. Furthermore, the behaviour of composite laminated plates and shell structures is influenced by the load history and the stress-strain field retained by the structure.

A significant amount of research has been conducted on the analyses of laminated anisotropic cylindrical shells subjected to stable static loading and buckling analyses of such shells. A review of various studies on the analysis of laminated shells is given by Bert and Francis [2], Leissa [8] and Kapania [7]. Apparently the first analysis as such was due to Cheng and Ho [3], who derived the buckling characteristic equation for cylinders subjected to combined axial compression, external pressure and torsion. Although their analysis is rather lengthy, it is based on a very accurate Flugge-type shell theory [4]. Their general analysis was later applied to obtain numerical results for buckling under various kinds of loading.

Due to its versatility, the finite element method is increasingly being used in the analysis of laminated shells. Detailed information on finite element and closed form theoretical investigations and experimental results can be found in ref [1]. In the present investigation, a widely finite element code, ABAQUS [6] was used. The finite element analysis was prompted to compare results obtained from experiments and a closed form solution.

THEORETICAL CONSIDERATIONS

Anisotropic Elastic Constants

In general a [6x6] elasticity matrix (with 36 constants) is required to specify an anisotropic material. However, on the basis of the existence of a unique and single valued elastic potential for a deformed structure, it can be shown that the elasticity matrix is symmetric and hence the number of constants required to characterise the material behaviour reduces to 21. The general transformation [9] of the sets of anisotropic elastic constants from one orthogonal Cartesian co-ordinate system to another with a different orientation is lengthy but straightforward. The transformation from an unprimed Cartesian co-ordinate system (x,y,z) to a primed co-ordinate system (x',y',z'), based on an elastic potential V in matrix notation is:

$$V = \tfrac{1}{2} [\varepsilon]^T \{\sigma\} \qquad 2.1$$

in the unprimed co-ordinate system; and:

$$V = \tfrac{1}{2} [\varepsilon']^T \{\sigma'\} \qquad 2.2$$

in the primed co-ordinate system.

The corresponding Hooke's law in the two systems of co-ordinates are:

$$\{\varepsilon\} = [c]\{\sigma\} \qquad 2.3$$

and

$$\{\varepsilon'\} = [c']\{\sigma'\} \qquad 2.4$$

Since stress is a second tensor quantity, its transformation from (x,y,z) to the (x',y',z') coordinate system (with the latter being oriented to the former with a_{ij} direction cosines, for (ij = 1,2,3):

$$\sigma'_{ij} = \sum\sum a_{im}\, a_{nj}\, \sigma_{mn} \qquad 2.5$$

Using equations 2.3 and 2.4 in equations 2.1 and 2.2 and equating the results we obtain:

$$\tfrac{1}{2}[\sigma]^T [c]^T \{\sigma\} = \tfrac{1}{2}[\sigma']^T [c']^T \{\sigma'\} \qquad 2.6$$

Using the stress transformation given in equation 2.5, in equation 2.6 and equating the coefficients of the corresponding quadratic stress components, the required transformation of elasticity matrix from one set of Cartesian co-ordinates to another is complete.

Failure of a Laminate Structure Under Impulsive Loading.

When a laminated composite is subjected to a loading in excess of its strength, it develops matrix cracks, fibre-matrix debonds, fibre fractures and/or delaminations. These effects, which cause permanent loss of integrity within the laminate, as in impact loading, are termed "damage" and they impair the service functionality of the structure. As a result, the load carrying capacity is diminished and the anticipated service life of the structure cut short. Under such circumstances it is accepted that the structure has failed. To predict failure various criteria have been postulated and a brief but adequate discussion of the different hypotheses is summarised by Ochoa and Reddy [10]. There are very many failure criteria and here we present the polynomial failure criterion proposed by Tsai-Wu [11]. All other polynomial failure

criteria are degenerate cases of this one. In index notation, the tensor polynomial failure criterion is expressed as:

$$F_i\,\sigma_i + F_{ij}\,\sigma_i\,\sigma_j + F_{ijk}\,\sigma_i\,\sigma_j\,\sigma_k + \ldots\ldots \geq 1 \qquad 2.7$$

or, in more explicit form

$$F_i\,\sigma_{11} + F_2\,\sigma_{22} + F_3\,\sigma_{33} + 2\left(F_{12}\,\sigma_{11}\,\sigma_{22} + F_{13}\,\sigma_{11}\,\sigma_{33} + F_{23}\,\sigma_{22}\,\sigma_{33}\right) +$$
$$F_{11}\,\sigma_{11}^{\,2} + F_{22}\,\sigma_{22}^{\,2} + F_{33}\,\sigma_{33}^{\,2} + F_{44}\,\sigma_{23}^{\,2} + F_{55}\,\sigma_{13}^{\,2} + F_{66}\,\sigma_{12}^{\,2} \geq 1 \qquad 2.8$$

where

$$F_i = \frac{1}{\sigma^D{}_{iT}} - \frac{1}{\sigma^D{}_{ic}} \quad for \quad i = 1,2,3 \quad , \quad F_{ii} = \frac{1}{\sigma^D{}_{iT}\,\sigma_{ic}} \quad for \quad i = 1,2,3$$

$$F_{44} = \frac{1}{\sigma^D{}_{23}\,\sigma^D{}_{23}} \quad , \quad F_{55} = \frac{1}{\sigma^D{}_{13}\,\sigma^D{}_{13}} \quad and \quad F_{66} = \frac{1}{\sigma^D{}_{12}\,\sigma^D{}_{12}}$$

$$F_{12} = -\tfrac{1}{2}\sqrt{F_{11}\,F_{22}} \quad , \quad F_{13} = -\tfrac{1}{2}\sqrt{F_{11}\,F_{33}} \quad and \quad F_{23} = -\tfrac{1}{2}\sqrt{F_{22}\,F_{33}}$$

with positive values for all σ_{ic}. This risk parameter for ply fabric using the Tsai-Wu criterion is defined as follows:

$$\lambda_{TSWU} = \frac{1}{K_1 \pm \sqrt{K_2}}$$

$$where, \quad K_1 = \frac{-K_3}{2\,K_4} \quad , \quad K_2 = K_1^{\,2} + \frac{1}{K_4} \quad , \quad K_3 = F_1\,\sigma_{11} + F_2\,\sigma_{22} + F_3\,\sigma_{33}$$

$$K_4 = 2\left(F_{12}\,\sigma_{11}\,\sigma_{22} + F_{12}\,\sigma_{11}\,\sigma_{33} + F_{23}\,\sigma_{22}\,\sigma_{33}\right) + F_{11}\,\sigma_{11}^{\,2} + F_{22}\,\sigma_{22}^{\,2} +$$
$$F_{33}\,\sigma_{33}^{\,2} + F_{44}\,\sigma_{23}^{\,2} + F_{55}\,\sigma_{13}^{\,2} + F_{66}\,\sigma_{12}^{\,2}$$

then for	$\lambda_{TSWU} < 1$	*no ply failure*
	$\lambda_{TSWU} = 1$	*first ply failure*
	$\lambda_{TSWU} > 1$	*ply failure*

BUCKLING ANALYSIS

The finite element method [6] is employed to examine the elastic buckling of 3 covers, with two plies per cover of (+5/-5°) fibre orientation of carbon fibre reinforced plastic cylindrical shell subjected to dynamic external pressure pulse [1]. The pressure wave generated is transmitted through the water filled space confined by the outer surface of the tube specimen and two rigid end plugs. The current analysis assumes that the pressure front loads the outer tube surface instantaneously on arrival and its load-time history is inputed in input file.

Modelling

The implementation of a finite element procedure is depicted in a chart (Figure 1) which include model discretisation, material property definition, boundary and constraint condition specification, load-time history definition, mesh convergence studies, finite element analysis phase(s) and post processing, presentation and interpretation of results.

Mesh generations

The model employed in the analysis is shown in Figure 2. Solution are computed for a thin walled model cylinder made of orthotropic multilayered material. The approach adopted is to treat the whole cylinder as a balanced angle ply laminates, having one stacking sequence throughout. In the study, the cylinder is constructed of 6 layers (3 cover tube) of carbon fibre reinforced plastic material each with thickness of 0.21 mm. The layers have alternate helical winding orientation of $\pm 5^{\circ}$, the angle of the winding with respect to the loading direction. The cylinders were 70 mm long with an inner diameter of 100 mm. Due to symmetry only half of the cylinder is modelled (Figure 2).

The surface of the cylinder is discretised and composed of 336 4-noded (SR4) shell elements (48 in the circumferential and 7 in axial directions). The chosen element has six degrees of freedom per node (three in translation and three in rotation) and so there are 24 degrees of freedom per element.

An axisymmetrical rigid surface, representing the flange was also generated and the model is shown in Figure 2. A frictional coefficient of 0.1 is assumed between the contacting surfaces.

Material Properties.

For each layer the following properties [1], based on static testing in the principal direction were used.

E_{11}= 138 MPa, $E_{22} = E_{33}$ = 8.4 GPa
$G_{12} = G_{13}$ = 5.19 GPa, G_{23} = 2.8 GPa
$\upsilon_{12} = \upsilon_{13}$ = 0.28, $\upsilon_{21} = \upsilon_{31}$ = 0.017, $\upsilon_{23} = \upsilon_{32}$= 0.50

where E_{11}, E_{22}, E_{33} are direct elastic moduli; G_{12} , G_{13} , G_{23} are shear moduli and υ_{12} , υ_{23} , υ_{31} are Poisson's ratio.

Loading.

In the analysis, the composite tube was loaded by applying a prescribed loading steps. The steps were specified according to the initial step size, the desired number of iteration per increment, and the maximum step size allowed in any increment.

Two steps in the solution were performed. In the first step a hydrostatic loading was applied to the system. In the second, a dynamic loading of a prescribed pressure-time was given to the system. In hydrostatic loading, only one load case is considered and the buckling strength of the specimens are evaluated. In dynamic loading, each run employs a prescribed load-time obtained experimentally [1].

RESULT AND DISCUSSION

A 3 cover carbon fibre reinforced plastic hoop wound tubes was subjected to an external impulsive loading of 12.24 MPa. In this case the model having 6 plies is shown in Figure 2. In this section under the prescribed loading condition, the system response is selected along the line from node 1 to 85 (in steps of 12). Figure 3 shows the cross-sectional view of deformation and deformed shape of the tube sequence at different time intervals. Figures 4 and 5 present the circumferential or hoop strains (E_{11}) and axial strains (E_{22}) respectively, at inner and outer surface. The associated average inside and outside strains and strain rates are presented on the same figure. The strain readings were taken at selected node number (node 1 to 85 in steps of 12) and on the longitudinal plane of symmetry at 45° intervals.

As the first step was taken, at a time interval of 42.5 μsec, the structure behaves linearly. After several increments, the circularity of the mid-plane is no longer maintained which appeared at the end of increment 36 (553 μsec) at a strain

level of 0.2 % approximately. The first sign of instability, however, occurred during increment 40 (605 μsec), when the strain shown in a narrow band start to depart from each other (Figure 4). At this stage the experimental [1] and predicted results correlate well with each other and up to the onset of buckling. As the time is further increased, a buckled shape starts to develop to a circumferential mode number 4 which also agrees well with the closed form solution[1]. As the time elapse, the buckled shape grew steadily. At this point, although structurally intact, the tube had already failed. To note, failure could not be accomodated because of the lack of provision for automatic material strength degradation on commencement of failure and therefore the direct use of failure criteria such as Tsai-Hill and Tsai-Wu, etc, as a material failure predictor is not possible (at least in the current version of the code).

Figure 6 shows the hoop strain, axial strain and shear strain along the circumference; their corresponding stresses are given in Figure 7. It shows the variation of strains and their corresponding stresses along the circumferences.

CONCLUSION

Reasonable agreement was obtained between the analytical and experimental results in the buckling pressure and number of circumferential waves. The experimental buckling loads averaged approximately 10 % of the analytical prediction based on a Flugge-type shell theory.

In the finite element modeling of composites tubes subjected to impulsive loading, it is necessary to include physical shell imperfection to precipitate the buckling. The finite element analysis highlight the importance of including the correct initial imperfections where changes in the initial shape and load distribution imperfections produced noticeable changes in the solution.

REFERENCES

1. Ahmad, R., (1996) "Strain Rate Effect on Compressive and Tensile Properties of Carbon Fibre Reinforced Plastic (CFRP) Tubes", PhD Thesis, UMIST, Manchester, UK.

2. Bert, C.W. and Francis, P.H., (1974) "Composite Material Mechanics : Structural Mechanics", AIAA J., Vol 12, pp1173 – 1186.

3. Cheng , S. and Ho, B.P.C., (1963) "Stability of Heterogeneous Aelotropic Cylindrical Shells under Combined Loading", AIAA J., Vol. 1, pp892 – 898.

4. Flugge, W., (1962), Stresses in Shells, Springer-Verlag, Berlin

5. Hibbit, H.D., Karlsson, B.I. and Sorenson, K., (1994) ABAQUS Users and Theory Manuals, Version 5.4, HKS Inc., Rhode Island, USA.

6. Kappania, R.K. (1989) "A Review on the Analysis of Laminated Shells", Trans ASME, J. Pressure Vessel Technology, Vol. 111, pp88 – 96.

7. Leissa, A.W., (1985) "Buckling of Laminated Composite Plates and Shells Panels", Air Force Wright Aeronautical Lab., AFWAL-TR-85-3069

8. Lekhnitskii, S.G., (1963), Theory of Elastic of Anisotropic Elastic Body, San Francisco, California, Holden-Day.

9. Ochoa, O.O. and Reddy, J.N., (1993), Finite Element Analysis of Composite Laminates, Kluwer Academic Publishers.

10. Tsai, S.W. and Wu, E.M., (1971) "A General Theory of Strength for Anisotropic Materials", J. Composite Materials, Vol. 5, pp38 – 80.

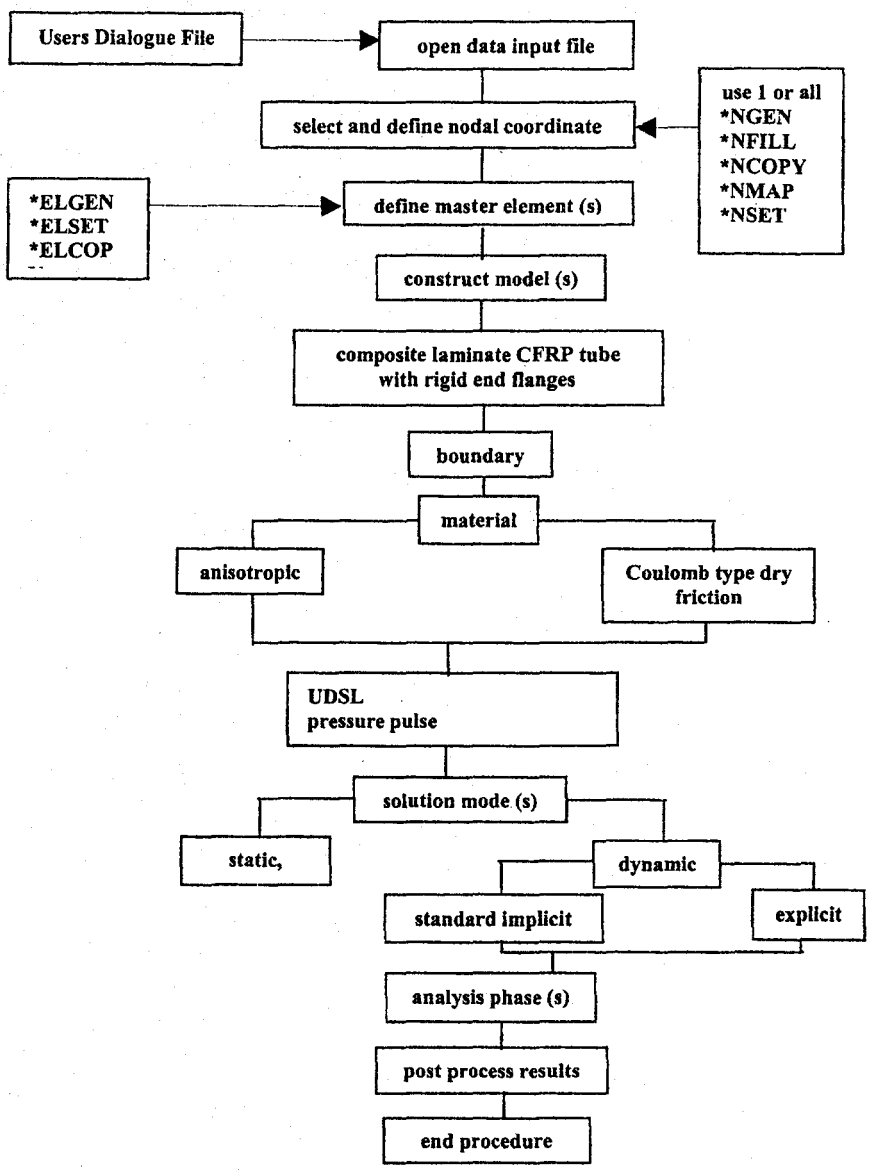

FIGURE 1 : Schematic solution procedure, model construction and analysis.

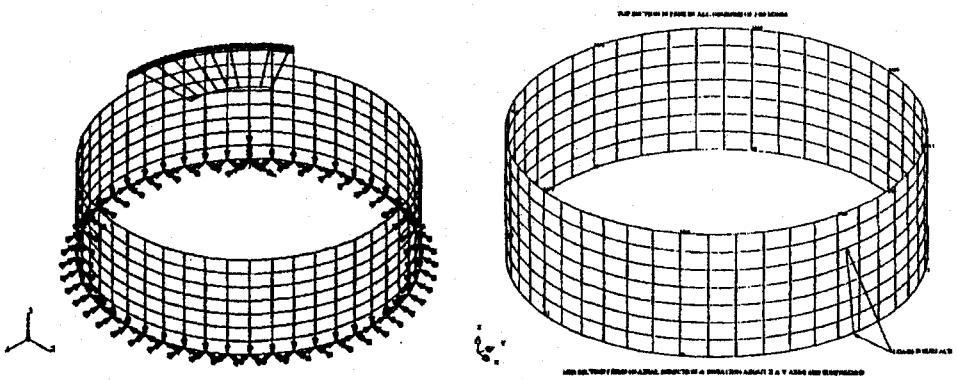

FIGURE 2 : Model in discretised from comprising of 336 4-noded (SR4) composite shell element with end flange

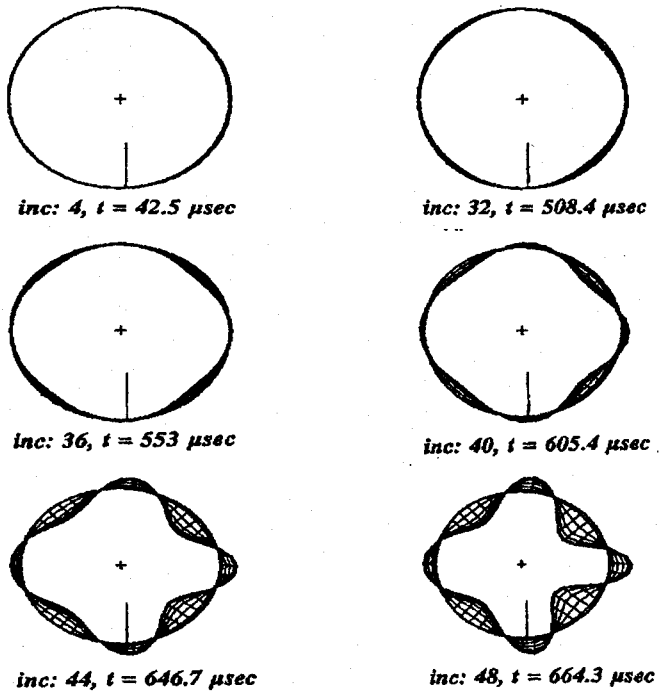

FIGURE 3 : Cross sectional view of deformed shape at mid plane of composite tube(3 cover) at various time in the loading sequence

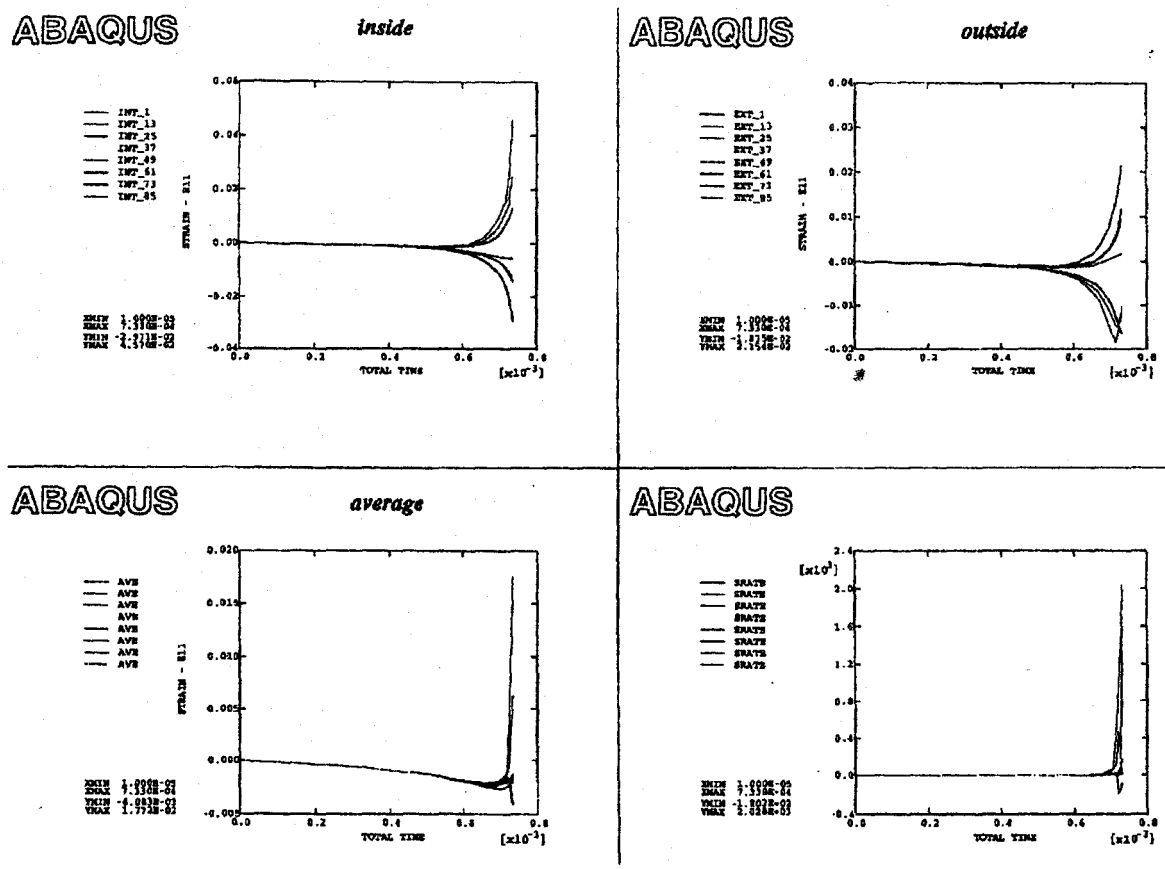

FIGURE 4 : Hoop strain (at inside, outside and average) time history and corresponding strain rate-time response at 45° interval for 3 cover CFRP tube.

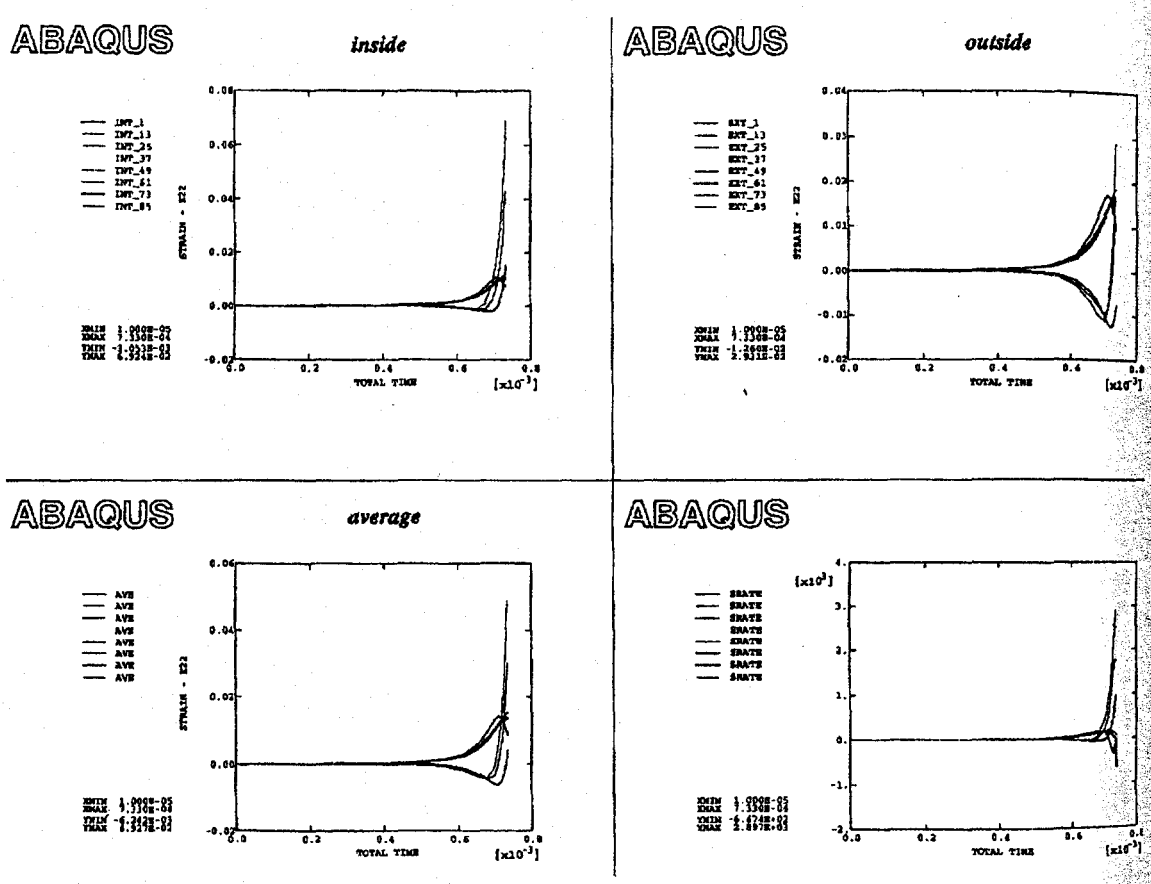

FIGURE 5 : Axial strain (at inside, outside and average) time history and corresponding strain rate-time response at 45° interval for 3 cover CFRP tube.

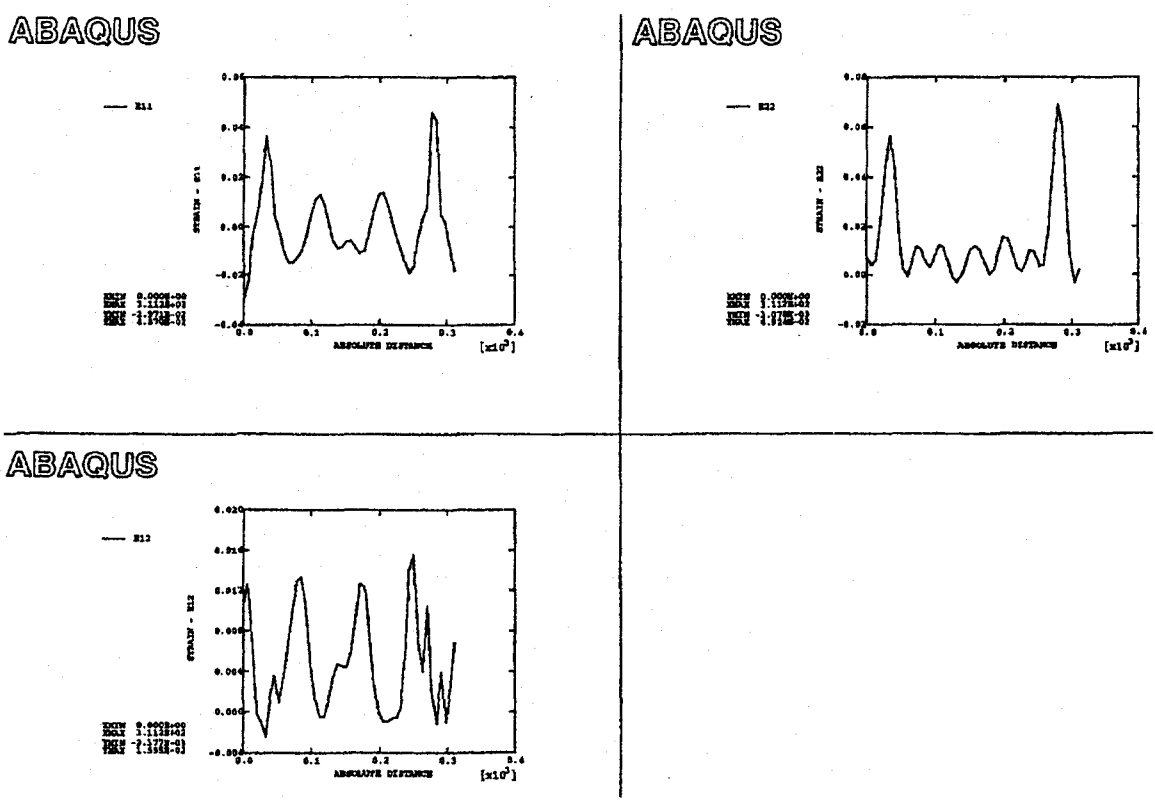

FIGURE 6 : Variation of average value of hoop, axial and shear strain along the tube circumference at t = 664.3 μsec.

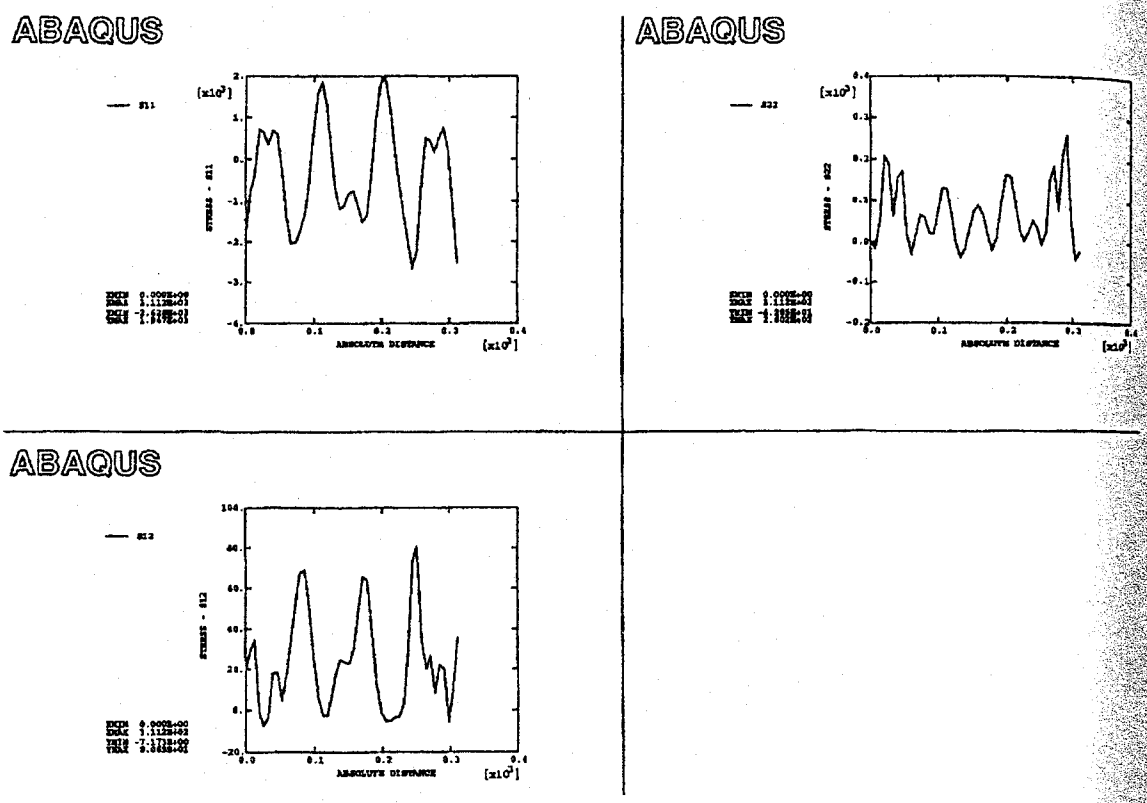

FIGURE 7 : Variation of average value of hoop, axial and shear stress along the tube circumference at t = 664.3 μsec.

4th International Conference on Mechanical Engineering, December 26-28, 2001, Dhaka, Bangladesh/pp. IV 31-36

THE EFFECT OF TURBULENCE INTENSITY ON THE AERODYNAMIC PERFORMANCE OF AIRFOILS

T.C.Yap*, M.Z.Abdullah,
Z.Husain, Z. Mohd Ripin, R. Ahmad
School of Mechanical Engineering, Universiti Sains Malaysia,
Engineering Campus, 14300 Nibong Tebal,
Pulau Pinang, MALAYSIA.

Abstract The experiments have been carried out in low speed, open circuit wind tunnel at the School of Mechanical Engineering, USM to study the effect of turbulence intensity on the airfoil's aerodynamic performance. Two types of airfoil i.e. NACA 0015 and Eagle 150 wing airfoils, are tested at three different Reynolds number. Three different density of wire-mesh are placed before the wind tunnel test section in order to generate turbulence in the range of 2.4% to 5.4%. The mean velocity and the turbulence intensity of the free stream flow are measured using a two-component Laser Doppler Anemometer (LDA). The results show that the increase in turbulence intensity delayed the stall angle but increased the lift and drag coefficients. The results obtained from the NACA 0015 and Eagle airfoil show almost similar trend. The results also show the stall is delayed with the increase of Reynolds number.

Keywords: Turbulence Intensity, Lift coefficient, Drag coefficient, Laser Doppler Anemometer

INTRODUCTION

Most of the aircraft and turbo-machine work in turbulent environment, the level of the turbulence will affect the flow's boundary layer separation. The aerodynamics characteristic of an airfoil is mainly depended on the flow characteristic (separation and reverse flow). As a result, the level of turbulent also affects the lift and drag coefficients of the airfoil. This information could help the designers and engineers to improve the performance of the aircraft or turbo machine.

Many investigators have studied the influence of turbulence to the separation bubbles in turbines blade aerodynamics and aerofoil performance. Hiller and Cherry (1981) have studied the effects of the stream turbulence on two-dimensional, separated and re-attached flows. They found that the mean flow-field responds strongly to the turbulence intensity but with little effect on integral scale and fluctuating pressures depend strongly upon both intensity and scale. However, the mechanism of turbulence interaction with the shear layer is unclear.

Butler et al. (2001) have studied the effect of turbulence intensity and length scale on low-pressure turbine blade aerodynamics. They found that for low Reynolds numbers (4.5×10^4-8×10^4), the boundary layer on the suction surface of the turbine blade always separated at lower turbulence intensity (0.4%-0.8%), increased the turbulence to a higher level (10%) could prevent the separation and the boundary layer transition to turbulent.

Mueller and Pohlen (1983) have studied the influence of turbulence intensity on the Lissaman 7769 airfoil. They have increased the nominal turbulent intensity from 0.08% to 0.30%, and tested at the Reynolds numbers below 3.0×10^5. They concluded that the increase in turbulent intensity could eliminate the hysteresis region, which occurs at the lift, and drag coefficients results. The increase in free stream turbulence and acoustic excitation also caused the laminar shear layer transformed into the transition region much earlier, thus allowing the flow to reattach.

Hoffmann (1991) has studied on the NACA 0015 airfoil at Reynolds number of $2.5\text{x}10^5$. The results show that the increasing in turbulent intensity from 0.25% to 9% has resulted 30% increased in maximum lift coefficient. At a higher turbulent intensity (9%), the maximum lift coefficient reached the saturation. The results also show that the increase in turbulent intensity increased the drag coefficient, however, the rate of change is negligible.

Huang and Lee (1999) had different results, they used NACA 0012 in their investigation and the Reynolds number ranged from $5\text{x}10^4$ to $1.4\text{x}10^5$. Huang and Lee only investigated turbulent intensity in the limited range of 0.2% to 0.65%. They found that the variation of lift and drag are closely related to the behavior of surface flow. The surface flow and L/D at low free stream

*Email: yaptc99@yahoo.com

turbulence are different from a higher free stream turbulence (>0.45%). The lift coefficient increased with the increase in turbulence intensity up to 0.45%. However, for the turbulence intensity higher than 0.45%, the lift coefficient decreased with the turbulence intensity. They concluded that the drag coefficient increases and the ratio of lift and drag coefficient decreases with the increase in turbulence intensity. At the lower turbulence intensity (less than 0.45%), the increasing of turbulence intensity has delayed the stall angle, however, at higher than 0.45% its influence is negligible.

EXPERIMENTAL SETUP AND PROCEDURE

The experiments are carried out in the low speed, open-circuit wind tunnel at the School of Mechanical Engineering, Universiti Sains Malaysia. The wind tunnel has a 300 x 300 x 600 mm Plexiglas's test section with three components electronic balance for the measurement of lift, drag and turning moment. The maximum velocity in the wind tunnel is 38m/s. The flow's mean velocity and the fluctuation values are measured by a DANTEC two component Laser Doppler Anemometer (LDA), and using a Spectra-Physics Model 177-G0232 with an air-cooled 300mW Argon ion laser as the light source. The two-component system used each the blue and the green laser light for both components. Signal analysis is obtained by a 58N40 Flow Velocity Analyzer enhanced processor and present in the FVA software. To measure the desired point more effectively, the laser probe is mounted on a traversing mechanism that can be controlled by the FVA software on the computer.

A smoke generator using the Shell ondina oil 15 is used as the seeding in this experiment. The smoke ejector is placed in front of the wind tunnel inlet to allow the smoke flow into the test section (Fig. 1). The purpose of this seeding is to allow the laser beam detect the flow velocity. The airfoils are made from fiberglass and both ends joined with plates, resulting in a rectangular box-shaped (bi-wing) assembly. One of the sides of the model is attached to a rod and connected to the wind tunnel's electronic balancing unit.

In order to generate different turbulence intensities in the test section, the mesh screen with different mesh density and wire diameter are put after the intake just before the test section. The mesh density, wire diameter and the turbulence intensity generated in the experiment at different Reynolds number are listed in Table 1.

In these experiments, the lift and drag forces of NACA 0015 and the Eagle's airfoils are investigated at three different Reynolds numbers i.e. $Re=6.4x10^4$, $1.27x10^5$ and $1.91x10^5$ corresponding to three free stream velocity of 10m/s, 20m/s and 30m/s respectively. Four different turbulence intensities are generated in the experiments and tested at various angles of attack from 0 to 15°.

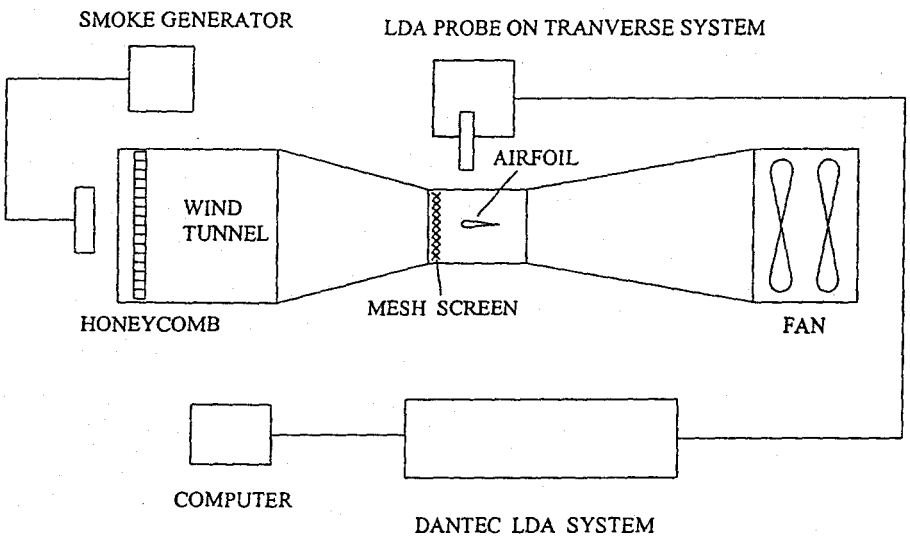

Fig. 1: Experimental Setup

RESULTS AND DISCUSSION

NACA 0015 Airfoil

Fig. 2 shows the variation of lift coefficient with respect to angle of attacks of NACA 0015 airfoil at a Reynolds number of $6.4x10^4$. At the lowest turbulence intensity of 2.45%, the lift coefficient is increased (increment rate ≈

1.67π/rad) with the increase of the angle of attack up to the stall angle (9°). After the stall angle, the lift coefficient dropped rapidly. Fig. 2 also shows that the increasing in the turbulent intensity causes the stall angle occurs at the higher angle of attack, and also increases the maximum lift coefficient. This is probably due to the increase in turbulent kinetic energy produced at the boundary layer with the higher energy on the airfoil which delayed the flow separation. When the stall angle occurs at a higher angle of attack, the lift coefficient reaches a higher value of C_{lmax}. The effect of the turbulence intensity on the drag coefficient for NACA 0015 airfoil is shown in Fig. 3. The result show that at Re= $6.4x10^4$, the increase in turbulence intensity caused small increase in the drag coefficient. The result also shows that the drag coefficient increases slowly with the increase in the angle of attack (increment rate ≈ 0.12π/rad) until it reaches the stall angle, and at the stall point, the drag coefficient increased suddenly with a higher slope (≈1.27π/rad).

In Fig. 4 and 5 show the lift and drag coefficients against angle attack of NACA 0015 at different turbulent intensity for Re=$1.27x10^5$. The results show similar trends as obtained for Re=$6.4x10^4$, the lift and drag coefficients increase with the increase of the turbulence intensity.

Furthermore, Fig. 4 and 5 also show the stall angle at Re=$1.27x10^5$ is higher than the stall angle at Re=$6.4x10^4$ (in Fig. 2 and 3), it illustrates that the increasing of Reynolds number delayed the stall angle. The Fig. 6 and 7 show variation of lift and drag coefficients versus angle of attack at higher Reynolds number (Re=$1.91x10^5$), the stall angle is delayed by the increase in the Reynolds number and the turbulence intensity. The variation of maximum lift coefficient with the Reynolds number is shown in Fig. 8. The maximum lift coefficient is increased with the turbulence intensity; however, the rate of increment is not linear with the increment of turbulent intensity. The result shows that the increase in turbulent intensity increased the maximum lift coefficient, however, when the Re increases, the C_{lmax} does not increase as expected. The C_{lmax} decreases when the Re increased from $6.4x10^4$ to $1.27x10^5$, however, after Re=$1.27x10^5$, the C_{lmax} increases.

Table 1: Turbulence intensities at different mesh and Reynolds number

Mesh screen number	Mesh density (mesh/cm)	Wire diameter (mm)	Turbulence intensity at Re=$6.4x10^4$ (%)	Turbulence intensity at Re=$1.27x10^5$ (%)	Turbulence intensity at Re=$1.91x10^5$ (%)
No mesh	-	-	2.45	2.39	1.81
M1	1.081	0.9	3.03	3.14	2.80
M2	3.077	0.7	3.36	3.41	3.07
M3	0.769	4	5.39	5.27	-

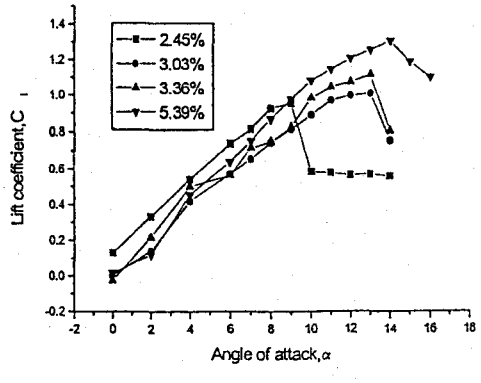

Fig 2: Lift coefficient versus angle of attack for NACA 0015 at Re = $6.4x10^4$.

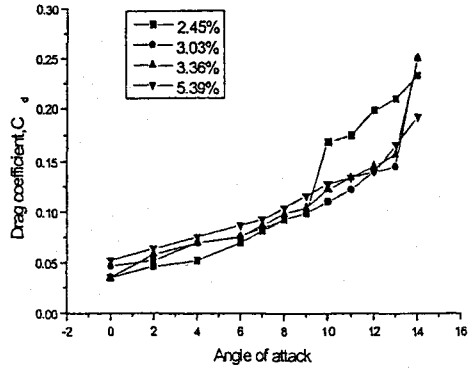

Fig 3: Drag coefficient versus angle of attack for NACA 0015 at Re=$6.4x10^4$

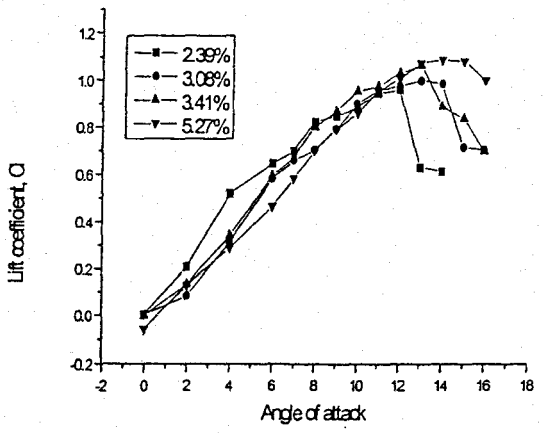

Fig. 4: Lift coefficient versus angle of attack Re= $1.27x10^5$ (NACA 0015)

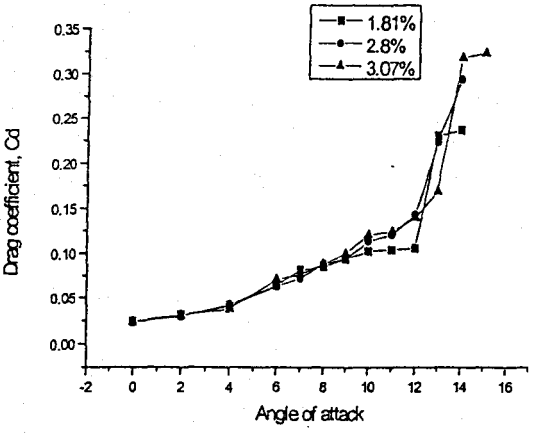

Fig. 7: Drag coefficient versus angle of attack at Re=$1.91x10^5$ (NACA 0015)

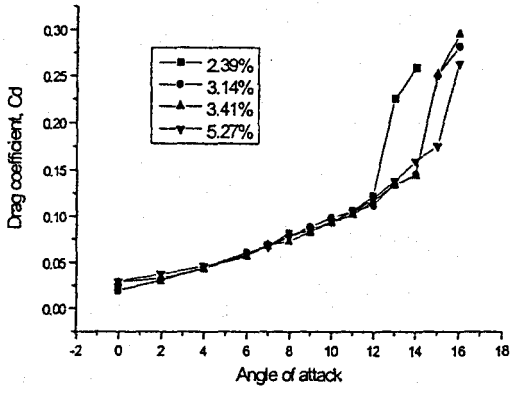

Fig. 5: Drag coefficient versus angle of attack at Re=$1.27x10^5$ (NACA 0015)

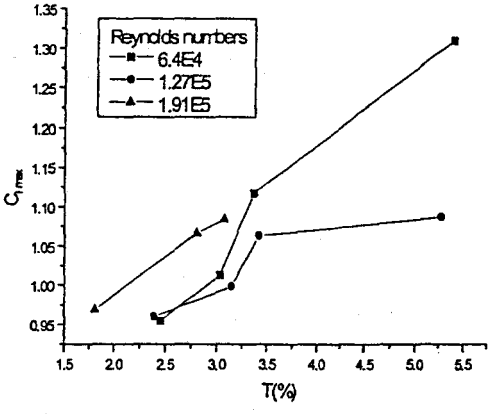

Fig. 8: Variation of maximum lift coefficient with Reynold's number

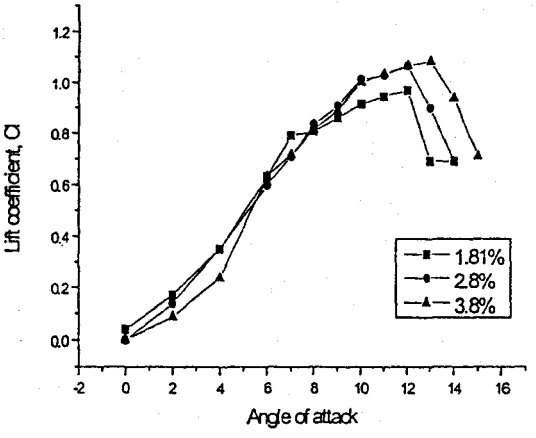

Fig. 6: Lift coefficient versus angle of attack at Re= $1.91x10^5$ (NACA 0015)

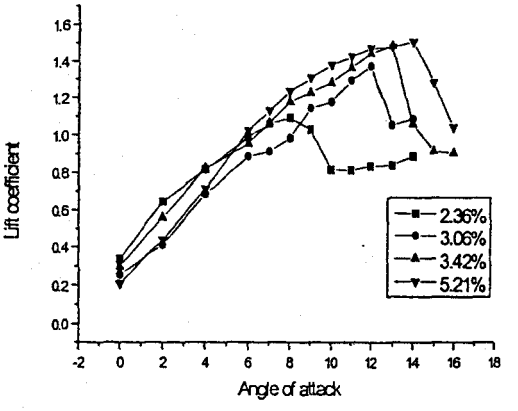

Fig. 9: Lift coefficient versus angle of attack of Eagle airfoil for Re=$6.4x10^4$

Eagle 150 wing airfoil

The results obtained from the Eagle airfoils are almost similar with the NACA 0015's airfoil. The Fig. 9 shows the relation between the lift coefficient and the turbulence intensity at various angles of attack. Generally, it shows that lift coefficient increases as the turbulent intensity increases.

The lift coefficient increases up to the stall angle and after the stall angle, the lift coefficient begin to decrease, however, the decrement rate is much slower than the slope of the NACA 0015 at the same situation. Fig. 10 shows the relation between the drag coefficient and the turbulent intensity at Re= 6.4×10^4. The drag coefficient also increases when the angle of attack increases. The results show the increment rate is small at the beginning, however, after the stall, the increment rate becomes steeper. This is mainly caused by suddenly increase in the pressure drag force due to flow separation.

The Fig. 11 shows the results of the lift coefficient at various angle of attack on Eagle 150 airfoil with three different turbulence intensity, Ti and at Reynolds number, Re=1.27×10^5. The stall angles are 9, 11 and 13° for the turbulence intensities of 2.54, 3.14 and 3.46% respectively. The results show that the increase in turbulence intensity resulted in delaying of the stall angle. Fig. 12 shows the drag coefficient of Eagle airfoil at different turbulence intensity versus the angle of attack. The results show that increase in the angle of attack resulted in a slight increase in the drag coefficient, and the drag coefficient increased suddenly at the stall angle. Fig. 13 and 14 show the results of the lift coefficient at the higher Reynolds number, Re= 1.91×10^5. At Re=1.91×10^5, the airfoil showed a similar trends as with the previous investigations. The increased of the turbulent intensity causes delay of the stall angle, and provided higher C_{lmax}. Fig. 14 shows that the increase of the turbulence intensity could increase the drag coefficient, however, the influence of the higher turbulence intensity to the drag coefficient is negligibly small. The slope of the drag coefficient perform almost constant until it reach the stall angle and than increased rapidly after the stall angle.

The variation of maximum lift coefficient, C_{lmax} with the turbulent intensity is shown in Fig. 15. At Re=6.4×10^4, the rate of increasing of C_{lmax} is almost linear (≈0.339) for turbulence intensity of 3.5%. However, the turbulence intensity above 3.5%, the increment rate becomes lower (≈0.011). At higher Reynolds number, Re= 1.27×10^5, the increment rate is about 0.345 and at Re=1.91×10^5 increment rate is 0.095. The results also illustrate that in order to increase the maximum lift coefficient, two methods could be used, either increase the turbulent intensity or increase the Reynolds number.

Comparison

In the investigations, two types of airfoil behave differently at different Reynolds number and influence of turbulence intensity has profound. The experiments show the results of lift and drag coefficients for both airfoils have similar trends at different turbulent intensity. In general for particular values of Reynolds number and turbulence intensity the Eagle airfoil has higher C_{lmax} compared to NACA 0015. The maximum lift curve of Eagle 150 airfoil is more stable compared to NACA 0015's.

CONCLUSION

The effect of turbulence intensity on the aerodynamics performance of the NACA 0015 and Eagle 150 airfoils is profound. The increase in air free stream turbulence intensity causes delay of the stall angle and the maximum lift coefficient. However, it causes the increase in drag coefficient.

ACKNOWLEDGEMENT

This study is supported by the IRPA long-term research grant provided by the Ministry of Science, Technology and Environment Malaysia. The authors also like to thank the National Science Fellowship (NSF) department for the financial support.

REFERENCES

Butler, R.J., Byerley, A.R., VanTreuren, K., and Baughn J.W., "The Effect of Turbulence Intensity and Length scale on Low-pressure Turbine Blade Aerodynamics", *International Journal of Heat and Fluid Flow, 22*, pp. 123-133 (2001).

Hillier, R. and Cherry, N.J. "The Effects of Stream Turbulence on Separation Bubbles", *Journal of Wing Engineering and Industrial Aerodynamics*, 8, pp. 49-58 (1981).

Hoffmann, J.A. "Effects of Free stream Turbulence on the Performance Characteristics of an Airfoil", *AIAA Journal*, 29(9), pp. 1353-1354 (1991).

Huang, R.F., and Lee, H.W. "Effects of Free stream Turbulence on Wing-Surface Flow and Aerodynamic Performance", *Journal of Aircraft*, 36(6), pp. 965-972 (1999).

Mueller, T.J., Pohlen, L.J., 1983, "The Influence of Free-Stream Disturbances on Low Reynolds Number Airfoil Experiments", *Experiments in Fluids*, 1, pp. 3-14 (1983).